
Theses and Dissertations

Fall 2010

Experimental verification of pointwise identification method for capturing heterogeneous properties in membranes

Brian Douglas Johns
University of Iowa

Follow this and additional works at: <https://ir.uiowa.edu/etd>



Part of the [Mechanical Engineering Commons](#)

Copyright 2010 Brian Douglas Johns

This thesis is available at Iowa Research Online: <https://ir.uiowa.edu/etd/824>

Recommended Citation

Johns, Brian Douglas. "Experimental verification of pointwise identification method for capturing heterogeneous properties in membranes." MS (Master of Science) thesis, University of Iowa, 2010.
<https://doi.org/10.17077/etd.st5j1yg7>

Follow this and additional works at: <https://ir.uiowa.edu/etd>



Part of the [Mechanical Engineering Commons](#)

EXPERIMENTAL VERIFICATION OF POINTWISE IDENTIFICATION METHOD
FOR CAPTURING HETEROGENEOUS PROPERTIES IN MEMBRANES

by
Brian Douglas Johns

A thesis submitted in partial fulfillment
of the requirements for the Master of
Science degree in Mechanical Engineering
in the Graduate College of
The University of Iowa

December 2010

Thesis Supervisor: Associate Professor Jia Lu

Graduate College
The University of Iowa
Iowa City, Iowa

CERTIFICATE OF APPROVAL

MASTER'S THESIS

This is to certify that the Master's thesis of

Brian Douglas Johns

has been approved by the Examining Committee
for the thesis requirement for the Master of Science
degree in Mechanical Engineering at the December 2010 graduation.

Thesis Committee: _____
Jia Lu, Thesis Supervisor

Geb Thomas

Olesya Zhupanska

ACKNOWLEDGMENTS

I would like to thank my advisor, Jia Lu, for consistent help in completing this thesis and continuous support through my graduate career. I would also like to recognize Geb Thomas for continual mentoring and teaching assistance throughout the past three years. Special thanks to my sister, Stacia Johns, for always being there and taking time out of her schedule to proofread my thesis. My sincere gratitude extends to all my friends and family who stood by my side during the good times, bad times and all the in-between times. Without these people I would not be where I am today.

TABLE OF CONTENTS

LIST OF FIGURES	v
CHAPTER 1: INTRODUCTION	1
1.1 Background	1
CHAPTER 2: TECHNICAL BACKGROUND.....	5
2.1 Pointwise Identification Method (PWIM)	5
2.2 Plane-Stress Membrane	7
2.3 Static Determinacy of a Membrane Structure.....	7
2.4 Constitutive Equation of Hyperelastic Materials	9
2.5 Kinematics of Membrane Deformation. The Cauchy-Green deformation tensor	11
2.6 Derivation of the Deformation Gradient	13
2.7 Derivation of Principal Stretches	17
2.8 Inverse Elastostatic Stress Analysis	19
CHAPTER 3: EXPERIMENTAL METHOD –RUBBER MEMBRANE TEST	21
3.1 Introduction.....	21
3.2 Experimental Setup	21
3.3 Camera and Environment Setup	22
3.4 Surface Preparation and Tracking Markers	23
3.5 Acquisition of Photographs	23
3.6 Processing of Photographs.....	24
3.7 Marker Correlation between Pressure States	25
CHAPTER 4 – RESULTS OF A RUBBER MEMBRANE TEST.....	26
4.1 Introduction.....	26
4.2 Stress Analysis Results	26
4.3 Strain Analysis Results.....	29
4.4 Correlation of Stress-Strain Results	30
CHAPTER 5 – DISCUSSION OF COMPLEXITIES IN BIOTISSUE TESTING.....	36
5.1 Introduction.....	36
5.2 Time Constraints	36
5.3 Surface Preparation	36
5.4 Camera Setup.....	38
5.5 Inflating the Bladder.....	38
CHAPTER 6: CONCLUSION.....	40
REFERENCES	42
APPENDIX A – MATHEMATICA CODE	44
APPENDIX B – MATLAB CODE.....	48
APPENDIX C – TECPLOT STRESS RESULTS	54
C.1 First Principal Stresses of Rubber Membrane Test	54
C.2 Second Principal Stresses of Rubber Membrane Test.....	57

APPENDIX D – TECPLOT STRETCH RESULTS	60
D.1 First Principal Stretches of Rubber Membrane Test	60
D.2 Second Principal Stretches of Rubber Membrane Test	63

LIST OF FIGURES

Figure 1. Pointwise Identification Method Flowchart.....	6
Figure 2. Convex Membrane Mesh Element.	7
Figure 3. Generic Stress-Strain Curve for Metals.	10
Figure 4. Hyperelastic Stress-Strain Curve of a Rubber-like Material (10).	11
Figure 5. Continuum Body Motion.	13
Figure 6. Membrane with Deformed Points.....	15
Figure 7. Mapping Vectors from 2D to 3D Space.	16
Figure 8. Diagram of Experimental Test Setup.....	22
Figure 9. Three Photographs of Inflated Balloon.....	24
Figure 10. Side-by-Side Comparison of 3D Reconstruction and Actual Photograph.....	27
Figure 11. First Principal Stress at Pressure State 14.	28
Figure 12. First Principal Stress Results at the lowest and highest pressure state.	28
Figure 13. First Principal Stretches at the Highest Pressure State.	30
Figure 14. Membrane Mesh showing coloration for stiffness of material.....	32
Figure 15. Sample: First Principal Stress vs. Principal Stretches.	33
Figure 16. Sample: Second Principal Stress vs. Principal Stretches.	34
Figure 17. Sample: Von Mises Stress vs. Average Principal Stretch.....	34
Figure 18. Sample: Overlaid plot of Nodes, Comparing Material Properties.....	35
Figure 19. Rabbit Bladder with Graphite Markers.....	37
Figure C1. First Principal Stresses, Pressure States 1 through 4.....	54
Figure C2. First Principal Stresses, Pressure States 5 through 10.....	55
Figure C3. First Principal Stresses, Pressure States 11 through 15.....	56
Figure C4. Second Principal Stresses, Pressure States 1 through 4.	57
Figure C5. Second Principal Stresses, Pressure States 5 through 10.	58
Figure C6. Second Principal Stresses, Pressure States 11 through 15.	59

Figure D1. First Principal Stretches, Pressure States 1 through 4.....	60
Figure D2. First Principal Stretches, Pressure States 5 through 10.....	61
Figure D3. First Principal Stretches, Pressure States 11 through 15.....	62
Figure D4. Second Principal Stretches, Pressure States 1 through 4.	63
Figure D5. Second Principal Stretches, Pressure States 5 through 10.	64
Figure D6. Second Principal Stretches, Pressure States 11 through 15.	65

CHAPTER 1: INTRODUCTION

1.1 Background

In recent years, there has been vast research in developing constitutive models for biological tissues. Constitutive equations simply define how much stress the material produces when subjected to a prescribed stretch. Stress responses are characterized experimentally using various methods based on which mathematical functions will be developed to delineate the stress-strain function. Due to the nature of the material, experimental validation of mathematical models in tissues poses a unique set of difficulties.

One complication of examining biological tissues is its nonlinear elastic properties, as opposed to linear elasticity. For example, a common metal spring exhibits linear elastic properties. If a weight hangs on a metal spring, it stretches to a certain length. If the weight is doubled, the spring would stretch twice the original distance. Alternatively, tissues exhibit non-linear elasticity. Doubling the weight on tissues might stretch the material half, triple, or 5 times the original length. Tissues exhibit non-linear elasticity. Without a material model, it is impossible to accurately describe how far the tissue would stretch. Fung performed some of the first research in modeling nonlinear elasticity of tissues. Experiments consisted of simply hanging weight in tension from rabbit abdominal tissue and observing stress and strain data. From this data theoretical framework was completed to develop a model to fit the experimental data (1).

Material anisotropy becomes a concern when modeling materials. A common everyday material that exhibits anisotropic properties is wood. The elastic properties of the wood depend on the structure of the grain. Due to anisotropy in tissues, many models are dependent on the direction of fibers. Rodriguez et al. noticed an increase in anisotropy in an abdominal aorta aneurysm as the degeneration increased. The circumferential direction was noticed as the direction of the main increase in stiffness (2).

Halperin et al. also observed anisotropic material properties for contraction and passive stretching of myocardial tissue in canines (3).

Another difficulty in tissues is heterogeneity. The material properties of the tissue differ depending on the location of interest because tissues adapt to meet functional demands. It has been observed that highly loaded articular cartilage contains more proteoglycan content and less loaded cartilage contains more collagen content. The difference in loading conditions produces a difference in tensile modulus, which shows heterogeneity in the material (4). Heterogeneity contributes to different material models being developed for different regions of the tissue. This lack of homogeneity adds more complexity to the problem.

Material models can also differentiate from one test specimen to the next. This has an important implication in biomedical applications. A material model containing population mean material properties may not describe a specific subject. At this point, the golden standard of patient-specific models is simply not there. Currently, patient specific models tend to be cumbersome and labor intensive. Image-based analysis could also provide the means for characterizing material properties for non-invasive procedures. Future advancements in imaging and technology will someday make these feasible for patients on a day-to-day basis.

This study focuses on thin materials forming a membrane structure. Examples of this type of biological structure include bladders, aneurysms, and diaphragms. Membrane structures have some special properties that can aid constitutive characterization. One of the properties is static determinacy. Static determinacy means the stress can be computed by balance laws and geometry alone, without the use of material models. A common plane-stress statically determinant problem is a thin-walled spherical pressure vessel. If the thickness of the material is much less than the radius of the sphere and the vessel is in equilibrium, the stress can be derived from Newton's first

law of motion alone, neglecting material properties. The resulting hoop stress from a pressure, P , radius, r , and a thickness of t is,

$$\sigma = \frac{Pr}{2t}$$

Closed-form stress solutions can be found for axisymmetric thin shells. Lu, Zhou, and Raghavan introduced a method for computing stress in a nonlinear heterogeneous membrane without geometric symmetry. This method was applied to cerebral aneurysms (5). The method uses an inverse formulation (taking the deformed configuration as a given known, solve for the un-loaded configuration and, at the same time, the stress in the given deformed state). The stress state for an irregular convex membrane is solved by means of balance laws alone, without the use of accurate material properties. This eliminates the need to generate a material model for computation of stress.

Lu and Zhao further utilized the inverse elastostatics to develop the Pointwise Identification Method (PWIM) for characterizing membrane tissues (6). The method utilizes separately acquired stress and strain data to derive the stress-strain function locally at each material point. The stress data is computed using the inverse method, which enables solving for the stress without resorting to the material model in question. The strain data is derived from measured surface motion, using techniques, such as 3D-scanning, CT scans, and ultrasound. Hsu et al. used a similar photogrammetric setup in inflation testing of a membrane. The experiment consisted of three video cameras tracking markers along the surface. Through this method the research was able to extract strain data for a small group of data points (7). The PWIM characterizes the properties by solving regression problems at each point of interest using the acquired stress-strain

data. This lays the groundwork for identifying the heterogeneous nature throughout the membrane.

The primary goal in this research was expanding the PWIM to improve a camera-based surface motion acquisition by using automated marker tracing and to validate the method in heterogeneous membranes. The design of the experiment places tracking markers along the surface of the membrane. These tracking markers are photographed at various pressure states. The tracking markers provide material points that are used as nodes to reconstruct the membrane mesh in a virtual environment, thus providing the basis for stress analysis. The tracking markers are also correlated between different pressure states; this provides displacement of the markers from one pressure state to the next. Knowing the displacement of the markers from one state to the next provides the basis for measuring strain in the material. The end result verifies the pointwise identification method as a valid procedure in measuring stress-strain material properties.

CHAPTER 2: TECHNICAL BACKGROUND

2.1 Pointwise Identification Method (PWIM)

To further understand the developing research, one must go into detail about the Pointwise Identification Method. The method starts simple, by merely marking a surface of a membrane with round markers and then inflating the membrane to a specified pressure. The next steps dive into the heart of the PWIM. Photogrammetric software is used to reconstruct the surface of the membrane. Next, inverse stress analysis begins. At each pressure state, stress and strain data are collected. Separate strain and stress computations are made among the same pressure state. Next, a stress-strain curve is made for every point in the heterogeneous membrane. The curves can qualitatively show the difference between the material properties across the membrane. If necessary, the stress-strain curve can fit to a mathematical function to quantify the properties. A flowchart of the Pointwise Identification Method is shown in Figure 1.

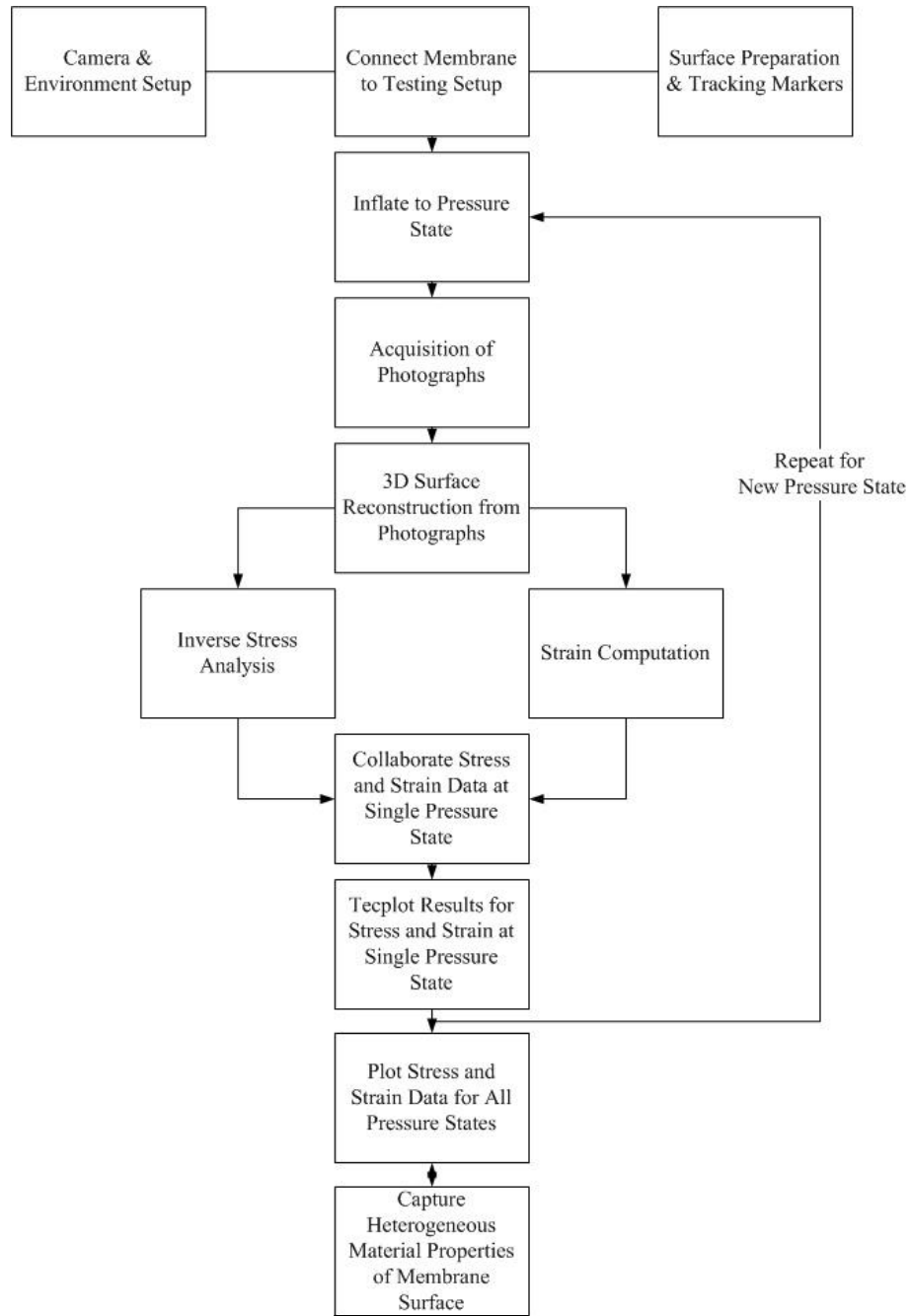


Figure 1. Pointwise Identification Method Flowchart.

2.2 Plane-Stress Membrane

Certain assumptions must be made about the characteristic behavior of the membrane in order to model the membrane material. Membranes are thin curved material sheets. During experimental testing the radius of the membrane was roughly 200 times larger than the thickness of the material. Transverse loads applied on the surface are sustained by in-plane stress by virtue of surface curvature. As a result, the membrane surface was modeled as a plane-stress condition which means, any normal or shear stress components perpendicular the midplane are assumed to be zero or negligible. A membrane sample element is shown in Figure 2.

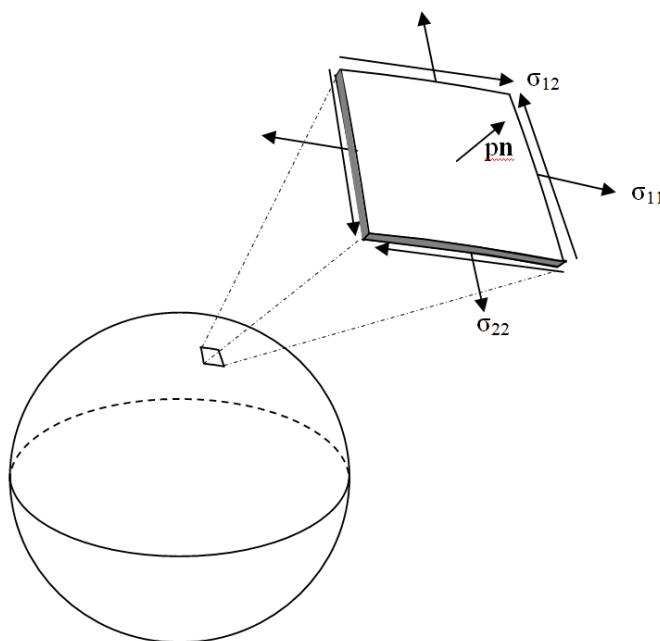


Figure 2. Convex Membrane Mesh Element.

2.3 Static Determinacy of a Membrane Structure

As mentioned previously, membrane stress computation is statically determinate, meaning the stress calculation is independent of the material properties. A common

plane-stress statically determinant problem is a thin-walled spherical pressure vessel, as mentioned in the introduction.

Figure 2 shows three components of stress: two normal stresses and one shear stress. Figure 2 also depicts the body force, p , caused by the internal pressure acting normal to the surface. The geometry of the curvature of the convex surface alone provides the basis for static determinacy. As the pressure pushes outward, the wall stress provides the pull to keep the membrane in equilibrium due to the curved nature of the membrane. The equilibrium equation becomes,

$$\text{div } \boldsymbol{\sigma} + p\mathbf{n} = 0.$$

If the equilibrium equation is expanded, three different non-linear differential equations result. These three differential equations can be used to solve for all three components of stress if the system is subjected to traction boundary conditions entirely. However, if a clamped or partially clamped boundary exists, the stress solution normally has a boundary layer effect, but the stress outside the boundary layer remains statically determined.

The beauty of the statically determinant problem is that the undeformed configuration does not influence the deformed stress computation. It may be difficult to imagine that the undeformed state does not affect stress. This can be best illustrated by example. If two thin-walled spherical pressure vessels are subjected to the same internal pressure and are geometrically identical when subjected to the pressure, and both have the same internal pressure and same geometric shape, the stress in both pressure vessels can be said to be equal. Although the pressure vessels have the same stress at a single state, one vessel could be made of steel, while the other is made of rubber. When deflated, the steel pressure vessel changes very little in geometric shape, whereas the deflated rubber pressure vessel shrinks to a very small shape. This example shows that the deformed stress is marginally dependent upon, (or even completely independent of)

the undeformed shape and the material. If the internal pressure and geometric shape are equal, the stresses will be equal. As a result, the pressure vessel could be made out of any material and yield the same stress state. This property still holds when the membrane is convex, and therefore, is not limited to spherical shaped vessels.

2.4 Constitutive Equation of Hyperelastic Materials

One goal of the experiment is to correlate stress data and stretch data. In metals, such as aluminum and steel, the elasticity is assumed to be linear to the point of proportional limit. That is, the strain of the material is assumed to be directly proportional to the stress of the material until the proportional limit is reached. The theory of linear elasticity is a cornerstone of fundamental deformable bodies. During linear elastic deformation of metals, the equation for tensile stress is Hooke's Law, $\sigma = E\varepsilon$. An approximate stress-strain curve for a metal is shown in Figure 3. The curve shows that the stress only varies linearly with the strain from the origin to the proportional limit (Point 2). Beyond the proportional limit, a different material model must be used to explain the stress-strain relationship.

Unlike metals, rubber does not follow linear elasticity from the beginning of deformation. Many rubbers can extend 300-500% without breaking, as opposed to mild steels, which will fail at only 25% elongation. The sub-microscopic make-up of the two materials explains the difference in elastic properties of the two materials. The molecules of a metal arrange carbon atoms in well-structured lattices, whereas the atomic structure of a rubber will look like a long tangled chain of carbon atoms, much like a clump of yarn. Rubbers will also possess the ability to rearrange carbon bonds during different deformations (8). Due to differences of the molecular makeup between metal and rubber it becomes apparent a different material model must be used to explain the stress-strain relationship.

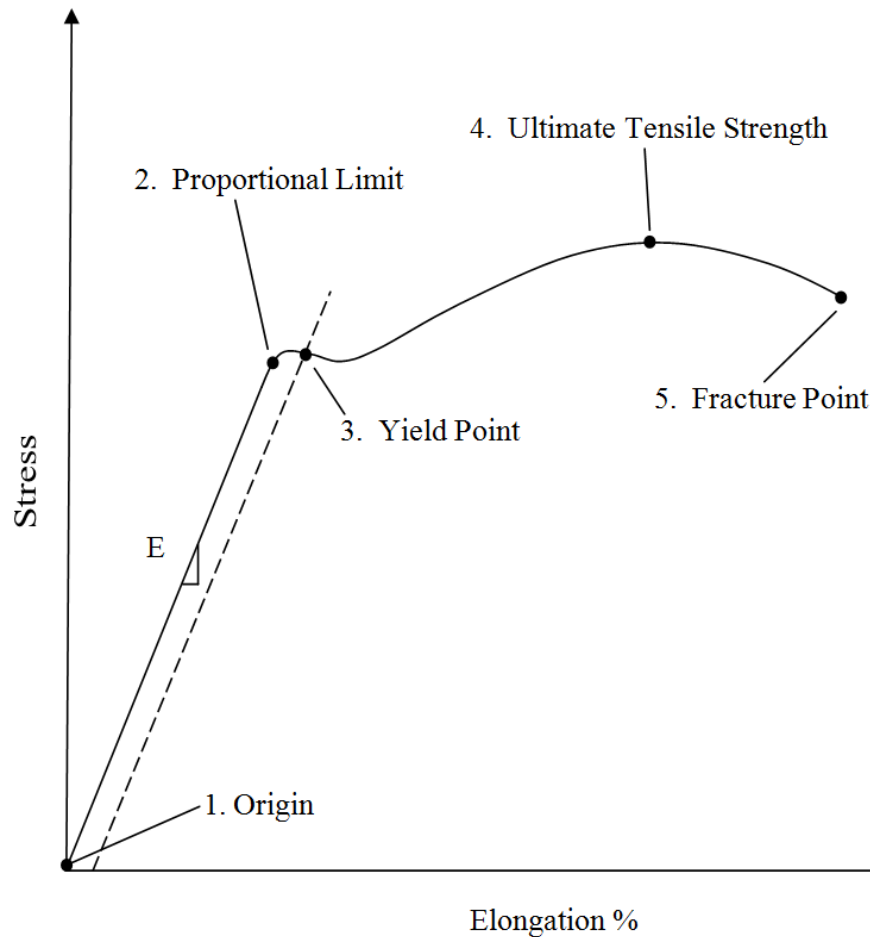


Figure 3. Generic Stress-Strain Curve for Metals.

The widely accepted constitutive model for rubbers and many tissues is known as hyperelastic material model. Hyperelastic models define the stress-strain relationship not as a linear model, but as a stress-strain relationship based on a strain energy density function. To qualitatively show the nonlinear behavior of hyperelastic materials, Figure 4 displays a generic stress-strain curve for a hyperelastic rubber-like material. A frequently used hyperelastic model is the neo-hookean model; the 2D membrane constitutive equation can be written as,

$$w(x) = \frac{v_1}{2} (I_1 - 2 \log J - 2) + \frac{v_2}{4} (I_1 - 2)^2.$$

The neo-hookean equation consists of two constant elastic parameters, v_1 and v_2 . The remaining unknowns are I_1 and J . The first invariant, I_1 , is simply $I_1 = \text{tr}(C)$, where C is the right Cauchy-Green deformation tensor. The Jacobian, J , is $J = \sqrt{\det C}$. By neglecting the two elastic constants, the constitutive equation proves to be only dependent on the right Cauchy-Green deformation tensor, C , therefore $w = w(C)$ (9).

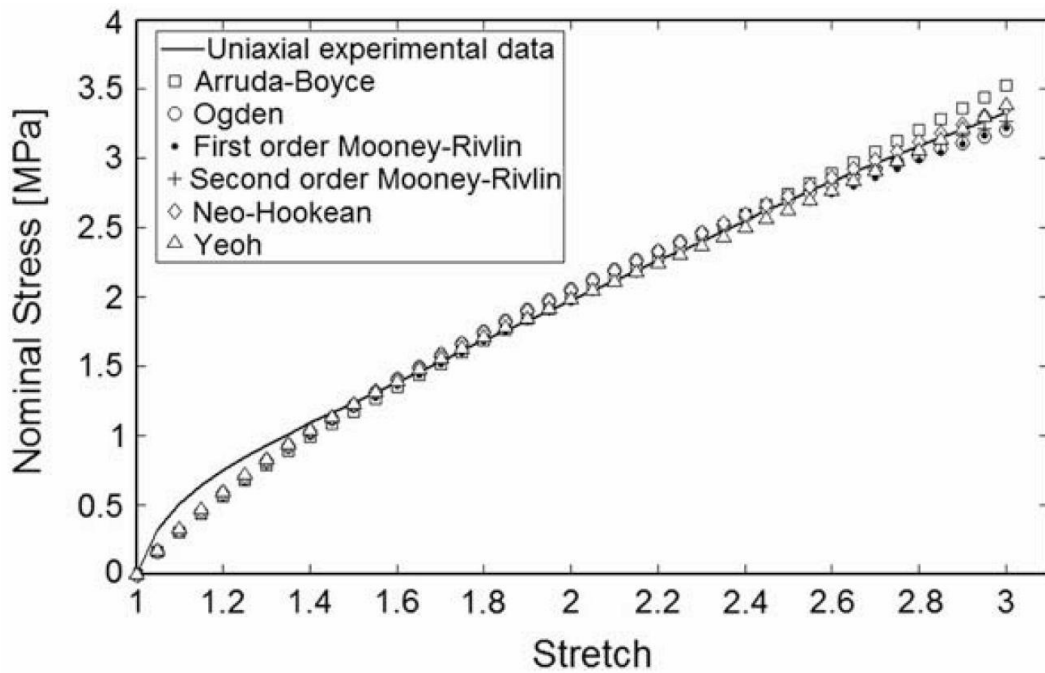


Figure 4. Hyperelastic Stress-Strain Curve of a Rubber-like Material (10).

2.5 Kinematics of Membrane Deformation. The Cauchy-Green deformation tensor

As shown above the object of interest is the right Cauchy-Green deformation tensor. To shed light on the physical meaning of the Cauchy-Green deformation tensor

take the following example modified from P.M. Naghdi's derivation (11). There are two points on the surface of a rubber material, \mathbf{P} and \mathbf{Q} . The vector that connects point \mathbf{P} to point \mathbf{Q} is defined as $d\mathbf{X}$. The rubber material is then stretched and rotated to another configuration. Point \mathbf{P} and point \mathbf{Q} represent the same points in the deformed state but are denoted as point \mathbf{p} and point \mathbf{q} , respectively. The vector that connects point \mathbf{p} and point \mathbf{q} is $d\mathbf{x}$. During the deformation, vector $d\mathbf{X}$ stretches and rotates to map to vector $d\mathbf{x}$. The tensor that maps the change is denoted \mathbf{F} , the deformation gradient. Therefore, the deformation equation becomes, $d\mathbf{x} = \mathbf{F} d\mathbf{X}$. A graphical interpretation of the change is shown in Figure 5.

The square of the magnitude of the deformed and undeformed vectors become, $dx^2 = dx_i dx_i$ and $dX^2 = dX_A dX_A$, respectively, where the subscripts indicate a summation over the indices. The difference of the squared magnitudes originally at \mathbf{P} and \mathbf{Q} becomes,

$$dx^2 - dX^2 = dx_i dx_i - dX_A dX_A.$$

By substituting the deformation gradient, $d\mathbf{x} = \mathbf{F} d\mathbf{X}$, the equation can be expanded as,

$$dx^2 - dX^2 = F_{ik} dX_A F_{kj} dX_B - dX_A dX_B.$$

Taking advantage of Kronecker delta, δ_{AB} , and the identity, $F_{ik} dX_A = dX_A F_{ki}$, the equation is simplified,

$$dx^2 - dX^2 = (F_{ki} F_{kj} - \delta_{AB}) dX_A dX_B.$$

This equation reaches the definition of the Cauchy-Green deformation tensor, \mathbf{C} ,

$$C_{ij} = F_{ki} F_{kj} \text{ or } \mathbf{C} = \mathbf{F}^T \mathbf{F}.$$

So,

$$dx^2 - dX^2 = (C_{ij} - \delta_{AB}) dX_A dX_B.$$

The above derivation of the Cauchy-Green deformation tensor proves that it is dependent only on the deformation gradient. As shown before the derivation, the neo-hookean strain energy density function was based solely on the deformation tensor. Thus, expanding the deformation tensor proves the neo-hookean material depends solely on the deformation gradient, \mathbf{F} . Therefore, $w = w(\mathbf{F})$.

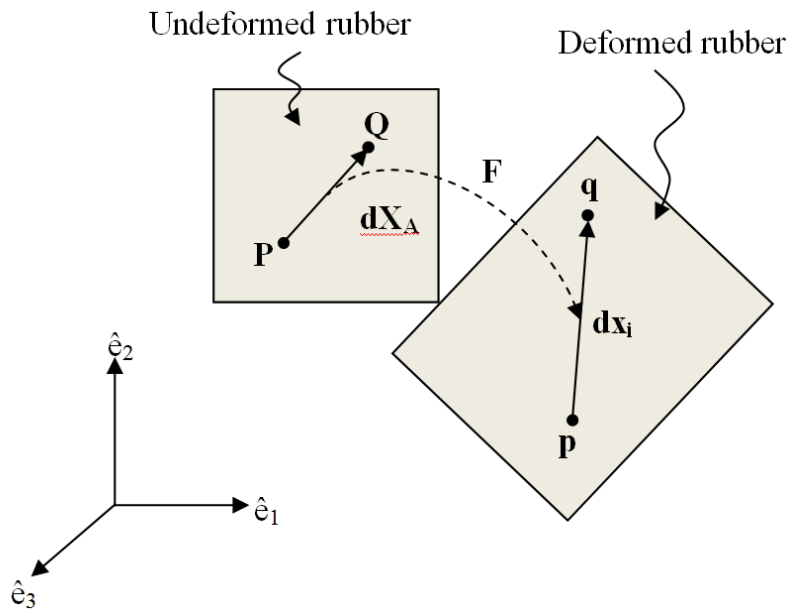


Figure 5. Continuum Body Motion.

2.6 Derivation of the Deformation Gradient

The pointwise identification method (PWIM) gives the basis for the deformation gradient. Each point on the surface of a membrane has a 3D coordinate in the reference configuration and a 3D coordinate in the deformed configuration. The neighboring

points in each configuration provide the endpoints for vectors. It then becomes possible to calculate to what degree the material stretches during the deformation, which yields the deformation gradient for each material point.

A graphical interpretation of the calculations presents a simplified explanation of how the deformation gradient is calculated. Assume three points, **P**, **Q**, and **R**, represent points on the surface of a reference configuration of a rubber membrane. The rubber membrane is then inflated, points **P**, **Q**, and **R** are stretched apart and become points **p**, **q**, and **r**, respectively, in the deformed configuration. The vector that connects point **P** to point **Q** is denoted as vector **A₁** and the vector that connects point **P** to point **R** is denoted **A₂**. The same relationship exists in the deformed configuration connecting the deformed coordinates, but the vectors are named **a₁** and **a₂**. This is shown graphically in Figure 6.

All vectors in the reference configuration and deformed configurations are formed in 3D vector space. A single 2D plane can contain both vectors, **A₁** and **A₂**, in the reference configuration. This plane is the tangent plane of the surface. A similar tangent plane can be made in the deformed configuration with vectors **a₁** and **a₂**. By using a local coordinate system which is tangent to the surface of the membrane, the problem is simplified as it becomes a 2D problem instead of a 3D problem.

An algorithm can be used to change the 3D vectors in the reference configuration to a 2D space. First take the cross product of vectors **A₁** and **A₂**, calling the result vector **B**,

$$\mathbf{A}_1 \times \mathbf{A}_2 = \mathbf{B}.$$

The cross product constructs a vector that is perpendicular to both vectors. The resulting vector, **B**, must be scaled to a unit vector. This can be done by dividing each component of vector **B** by the length of vector **B**. The resulting unit-vector is denoted **U**.

$$\mathbf{U} = \frac{\mathbf{B}}{\|\mathbf{B}\|}$$

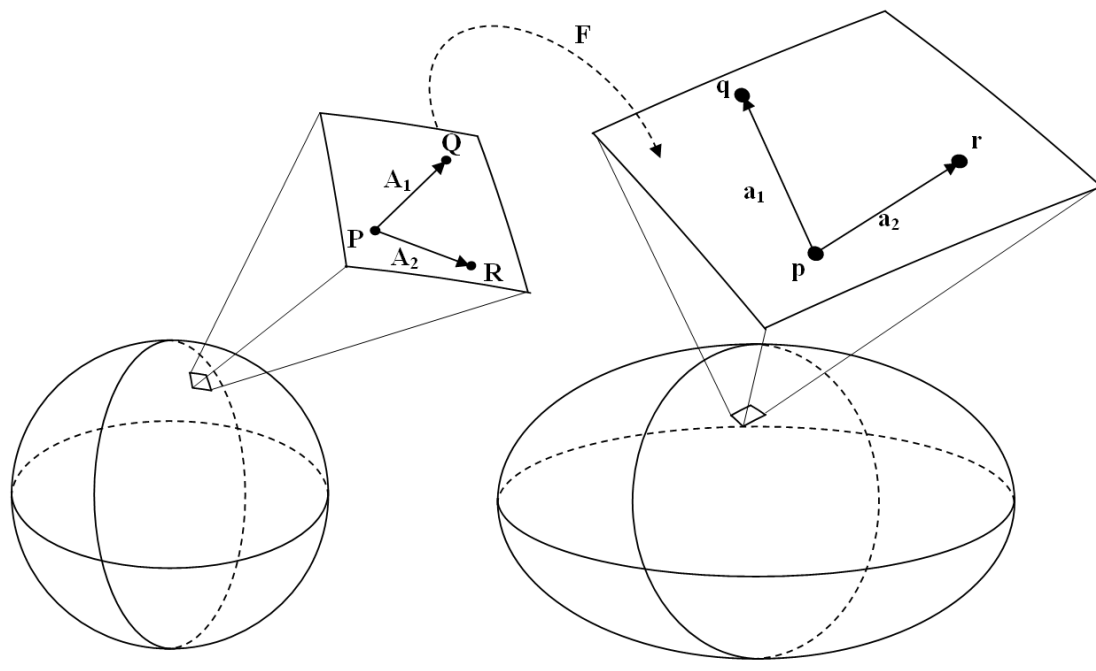


Figure 6. Membrane with Deformed Points.

Next, a rotation needs to be constructed that changes vector \mathbf{B} to be perpendicular to the x-y plane, which means \mathbf{B} needs to be rotated to point in the z-direction, i.e. the direction of vector $[0,0,1]^T$. The rotation matrix that points unit vector \mathbf{U} to the z-direction is labeled \mathbf{R}_{ref} . A graphical interpretation of the transformation is shown in Figure 7.

The rotation that maps vector \mathbf{U} to the z-axis is denoted as,

$$\mathbf{R}_{\text{ref}} \mathbf{U} = \begin{bmatrix} 0 \\ 0 \\ 1 \end{bmatrix} \text{ or } \begin{bmatrix} R_{11} & R_{12} & R_{13} \\ R_{21} & R_{22} & R_{23} \\ R_{31} & R_{32} & R_{33} \end{bmatrix} \begin{bmatrix} U_1 \\ U_2 \\ U_3 \end{bmatrix} = \begin{bmatrix} 0 \\ 0 \\ 1 \end{bmatrix}.$$

Next, it is necessary to solve for the rotation matrix, which includes 9 unknowns. With only three equations to solve for nine unknowns, another method must be employed to solve the rotation matrix. To make this equation solvable, it is possible to define the

rotation matrix in terms of Euler angles. Using a rotation around the Z-axis (ϕ), then the X-axis (Θ), then finally around the Z-axis (ψ) yields the Euler angle rotation matrix and the equation,

$$\begin{bmatrix} \cos \psi \cos \phi - \cos \Theta \sin \phi \sin \psi & -\sin \psi \cos \phi - \cos \Theta \sin \phi \cos \psi & \sin \Theta \sin \phi \\ \cos \psi \sin \phi + \cos \Theta \cos \phi \sin \psi & -\sin \psi \sin \phi + \cos \Theta \cos \phi \cos \psi & -\sin \Theta \cos \phi \\ \sin \Theta \sin \psi & \sin \Theta \cos \psi & \cos \Theta \end{bmatrix} \begin{bmatrix} U_1 \\ U_2 \\ U_3 \end{bmatrix} = \begin{bmatrix} 0 \\ 0 \\ 1 \end{bmatrix}.$$

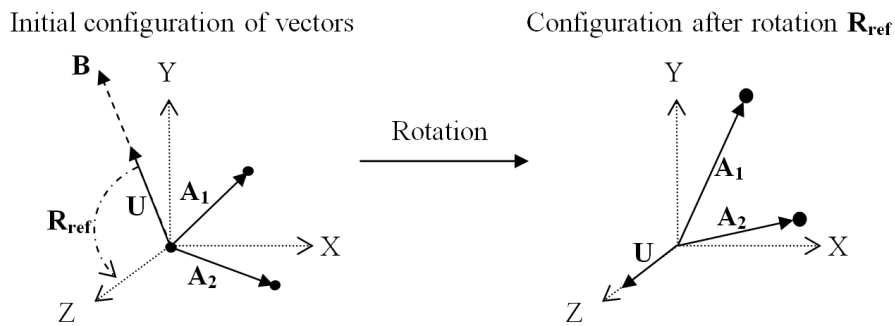


Figure 7. Mapping Vectors from 2D to 3D Space.

The equation results in a system of three linear equations with three unknown Euler angles which can be solved using a variety of methods. The same algorithm used previously is applied to the deformed configuration, mapping vectors \mathbf{a}_1 and \mathbf{a}_2 to a 2D coordinate plane. The rotation matrix for the deformed configuration is denoted \mathbf{R}_{def} .

Once both rotation matrices are defined for the reference and deformed states the deformation gradient, \mathbf{F} , can be derived. The reference vectors and the deformed vectors are multiplied by their respective rotation matrices to result in vectors that span 2D space. The 2D vectors are then denoted by \mathbf{V}_1 , \mathbf{V}_2 , \mathbf{v}_1 and \mathbf{v}_2 .

$$\mathbf{V}_1 = \mathbf{R}_{\text{ref}}\mathbf{A}_1 \quad \mathbf{V}_2 = \mathbf{R}_{\text{ref}}\mathbf{A}_2$$

$$\mathbf{v}_1 = \mathbf{R}_{\text{def}} \mathbf{a}_1 \quad \mathbf{v}_2 = \mathbf{R}_{\text{def}} \mathbf{a}_2$$

The resulting 2D vectors are then placed as columns in a matrix. The deformation gradient is then defined as the matrix which maps the reference configuration to the deformed configuration. The equation follows,

$$\mathbf{F}[\mathbf{V}_1 \quad \mathbf{V}_2] = [\mathbf{v}_1 \quad \mathbf{v}_2].$$

The deformation gradient, \mathbf{F} , is then solved by taking the inverse of the reference 2x2 vector matrix. The deformation gradient becomes,

$$\mathbf{F} = [\mathbf{v}_1 \quad \mathbf{v}_2][\mathbf{V}_1 \quad \mathbf{V}_2]^{-1}.$$

The deformation gradient becomes the key element when defining deformation in a continuum body. The deformation gradient can be implemented for each point through the entire membrane. Through the derivation, it is shown that the deformation gradient is solely dependent on the relative change of points compared to the reference state and is not dependent on the coordinate systems in either the reference or deformed configurations. It is also important to note the deformation gradient does not take into account the curvature of the membrane. If the curvature of the membrane changes rapidly in respect to the identification point spacing it will not accurately portray the deformation.

2.7 Derivation of Principal Stretches

Once the deformation gradient at a point is derived the calculation for material stretches can be derived. The stretch of a material is defined as the ratio of the deformed length to the original length (11).

$$\text{Stretch} = \frac{\text{deformed length}}{\text{original length}}$$

In the membrane, the most important factor is not necessarily how much a single line element stretches. It is more important to figure out the maximum stretch and minimum stretch of a point and the directions that a material stretches. The first step in finding the maximum and minimum stretch is deriving the Cauchy-Green deformation tensor at that particular point. This can be done once the deformation gradient is known,

$$\mathbf{C} = \mathbf{F}^T \mathbf{F}.$$

Once the deformation tensor is calculated at a material point, the principal stretches, can be found by finding the eigenvalues of tensor. The eigenvalues of the deformation tensor are the squares of the principal stretches, λ_1 and λ_2 .

$$(\mathbf{C} - \lambda^2 \mathbf{I})\mathbf{x} = 0$$

Since the deformation gradient is defined as a 2x2 matrix the Cauchy-Green deformation tensor is also a 2x2 matrix. The eigenvalues of a 2x2 symmetric matrix are derived as,

$$\lambda_1^2, \lambda_2^2 = \frac{C_{11} + C_{22}}{2} \pm \frac{\sqrt{4 C_{12}^2 + (C_{11} - C_{22})^2}}{2}.$$

It has been established that inverse stress analysis yields nonlinear differential equations. These equations must be solved simultaneously at every node. Solving the equations analytically involves a painstaking process even for a simplified axisymmetric homogeneous membrane. In the case of biological tissues, it is necessary to solve nonaxisymmetric heterogeneous membrane stress. Since an analytical solution to these tissues would be difficult to obtain a creative use of finite element method is exercised.

2.8 Inverse Elastostatic Stress Analysis

Often when solving a finite element problem the undeformed state is usually a known condition, such as the unloaded state of a beam. The solution becomes the deformation and stress when the beam is subject to boundary conditions and various loads. A method called forward analysis is used to solve for the deformed case when the undeformed condition is known. However, the case of the membrane is the inverse of the forward analysis situation because the undeformed state is unknown. This is because the photograph acquisition system collects data at each of the loaded states, but the original unloaded state is unknown. Therefore, the method of solving for the undeformed state is called inverse finite element method. One practical application of a known deformed shape and solving for the undeformed shape is gasket design. Govindjee and Mihalic explored the problem by knowing the deformed shape of the gasket needed to seal fluid and solving for the undeformed shape for the manufacturer (12).

As mentioned before the membrane stress is statically determinant, meaning the problem can theoretically be solved by the deformed shape alone. However, finite element is used to find a numerical solution to the stress instead to simplify the problem and cut computation time, which requires both an undeformed and deformed state to solve stress equations. This method is adopted from Zhou and Lu's formulation for inverse thin-walled structures (13). The finite element method solves problems via virtual work, and virtual work requires displacements to compute stresses. To obtain these displacements, the stress-free configuration is needed. As long as the undeformed shape is a stress-free configuration, it does not necessarily need to be an accurate representation of the deflated membrane. However, solving for the membrane's realistic undeformed shape may be impossible because most convex membranes will collapse without a load applied. Another situation exists when some materials, without an internal pressure, would be subjected to residual stresses, therefore a realistic stress free configuration would be impossible to obtain.

The undeformed stress-free configuration of the membrane is only sought after to adapt to the framework of finite element analysis. It does not affect the stress of the deformed membrane. The stress free configuration represents the mesh with no stresses present. To solve for stress in the membrane iteratively, the finite element code finds the stress-free configuration. When the load is applied to the solved stress free mesh, it then stretches into the deformed configuration detected by the motion acquisition system.

Since the material properties of the material do not affect solution in determining the wall stress, they are assumed to arbitrary values. For the rubber membrane a neohookean model was assumed with stiff material constants. The stiff material constants ensure quick convergence because the nodes from the deformed state will change minutely to the stress free configuration. As mentioned before, since the material model does not influence the stress, a material that yields quick convergence should be chosen to save computation time.

CHAPTER 3: EXPERIMENTAL METHOD –RUBBER MEMBRANE TEST

3.1 Introduction

The important elements in the experimentation are the accurate representation of the membrane surface and the tracking of surface points throughout the deformation history. Points are identified and tracked through the use of a camera. The science of reconstructing 3D models and geometric entities through photographs is known as photogrammetry. Photogrammetry is widely used crime scene reconstruction, geological terrain mapping, and also the film and animation industry (14). During the Pointwise Identification Method, photogrammetry was used to model the specimen surface and track strain through various pressure states. Capturing image data must be a quick and accurate system because most biological tissues dry out in a matter of minutes if the experiment is not completed in a timely matter. The use of a camera, or multiple cameras, generates the quickest way to capture the surface data at a certain pressure state.

Laser scans of membranes have also been used for 3D reconstruction of surfaces. This is a far superior tool when capturing an accurate surface, which results a more accurate stress state solution. However, the laser scanning cannot track points as they deform from one pressure state to the next. For example, a laser scan of a membrane generates a mesh of the surface for one pressure state, then by increasing the pressure in the membrane it deforms to a different state. Another laser scan mesh is created from the deformed state. An entirely new set of data points results in the loss of correlation of points between one scan to the next (15). For this reason photogrammetric techniques seem superior to enable extraction of stress-strain data from a membrane.

3.2 Experimental Setup

The schematic of the experimental setup is shown in Figure 8. The function of Components A-D in Figure 8 dropped the incoming air pressure from 90 psi to a pressure

range of 0-2 psi for the experiment. Component E was the test specimen, and Component F, the U-tube monometer, was used for internal pressure measurement. An advantage to this simplistic setup is that it can easily modify to accommodate many pressure ranges.

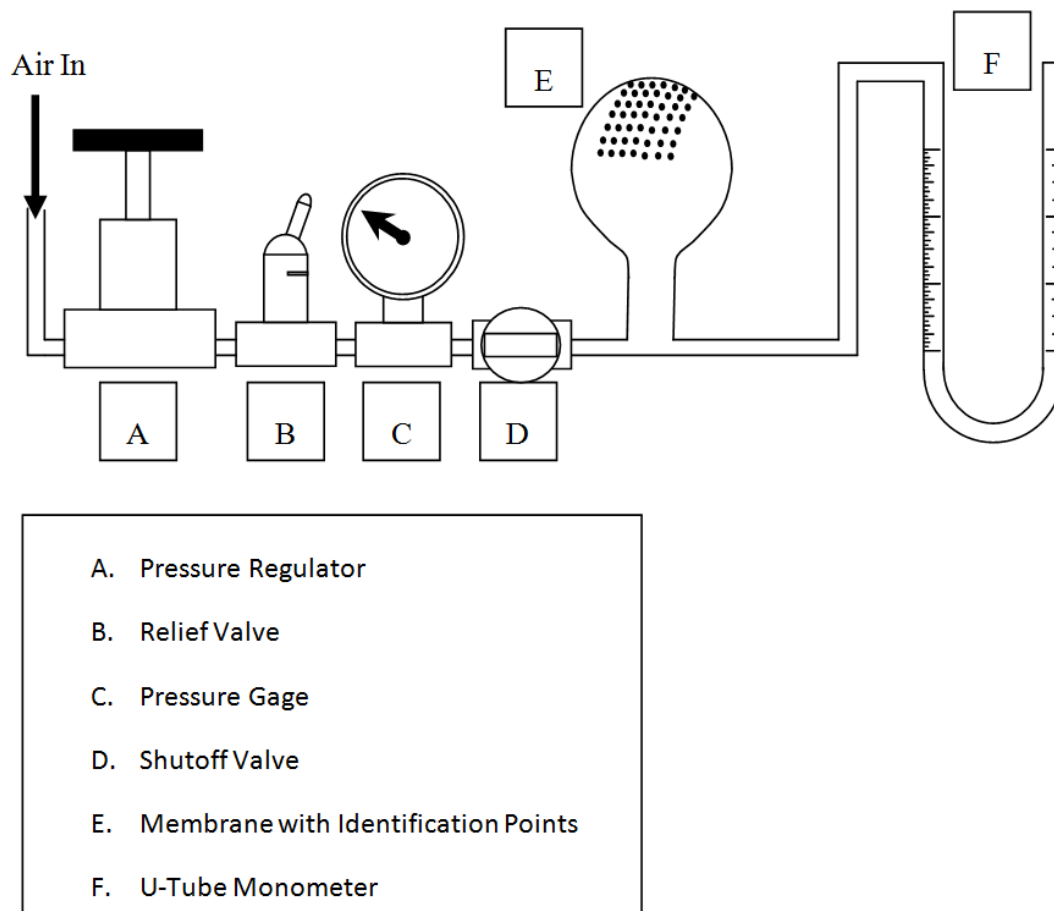


Figure 8. Diagram of Experimental Test Setup.

3.3 Camera and Environment Setup

Prior to setting up the membrane, the camera and surrounding area was set up to properly provide clear and precise photographs. A Nikon D80 10.2 megapixel camera

was used to capture the images. For small membrane experiments, there was difficulty capturing a large depth field identification points. To compensate for this problem, the aperture of the camera was adjusted to be very small. The small aperture, acting much like a pin-hole camera, brought all depths into focus, but posed the problem of insufficient light for each exposure. To resolve this difficulty, the exposure time was lengthened until adequate light was allowed into the camera. A four-second exposure time provided the sharpest photographs with $f/29$ aperture size.

3.4 Surface Preparation and Tracking Markers

Preparing the surface and placing tracking points on the surface proved to be a crucial step, and was also the most difficult. Identification points needed to be placed close enough together to capture the heterogeneity of the tissue. The tracking system was accurate if markers could be placed in an equally spaced array of points. However, if two markers came in contact, the point became unusable because the acquisition system could not properly identify the center of the marker. The simplest form of marking was placing a point on the surface using ink because this eliminated the need for manual marker identification.

The rubber membrane was the easiest surface for applying markers. The identification points were drawn onto the surface using a fine tip marker. Markers were arranged in a 19 x 21 row and column array amounting to a total of 399 identification markers. This well-ordered structure of points allowed for easier tracking in later steps.

3.5 Acquisition of Photographs

Once identification markers were made and camera calibrations completed the pressure states could be recorded. The rubber membrane was inflated and deflated numerous times to minimize Mullin's effect in the deformation. Next, the membrane was inflated to the highest pressure state and pressure was allowed to stabilize. Three

photographs were taken making sure all identification markers were in the view field. Each photograph was taken approximately 30 degrees from the previous photograph to enable accurate identification point location in 3D reconstruction. An example of three photographs taken at a single pressure state is shown in Figure 9.

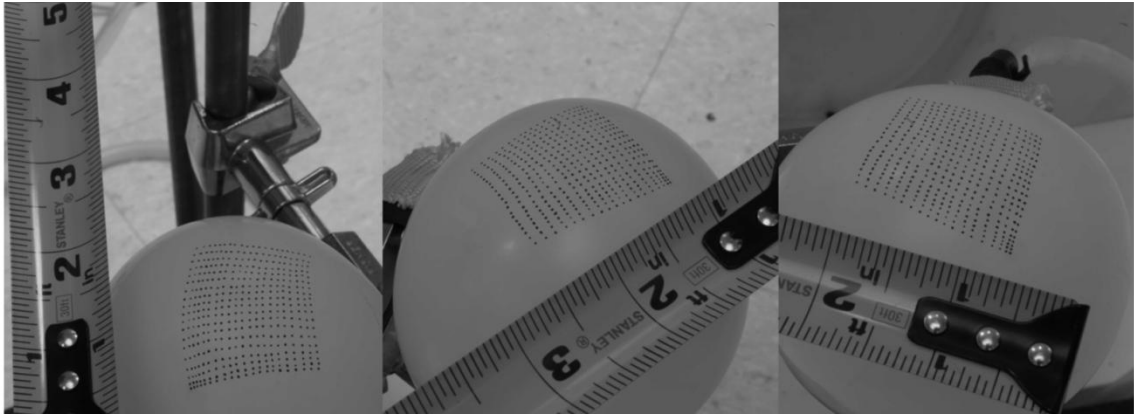


Figure 9. Three Photographs of Inflated Balloon.

Next, the pressure was deflated by approximately 0.01 psi and pressure was allowed to settle again. Three photographs were taken at the new pressure state. This process of deflation and photographs was repeated until the rubber membrane was close to nearly deflated, resulting in photographs from fifteen different pressure states.

3.6 Processing of Photographs

The first stage of photograph processing begins with importing the three photographs for each pressure state into Photomodler (Eos Systems). The software begins by setting up a point-based project. In all three photographs, identification markers were automatically identified by specifying an approximate size, circularity, and darkness of identification points on the membrane. Next, five of the identification points

were correlated between each photograph using manual selection, a minimum requirement for solving the camera locations.

Next, camera locations were identified and the automatic referencing tool was used. The automatic referencing tool uses ray lines from camera locations to correlate identification points from one photograph to the next photograph. This tool saved the task of correlating each point manually. However, without small distances between identification points and an organized point layout, automatic referencing fails. In this random point layout, such as sprinkled graphite on a membrane, referencing failed and required manual correlation of all points. After references were made, a known distance between points was used to scale the project and a universal coordinate system was picked. In the rubber membrane experiment, 399 points were correlated in each pressure state. The use of more correlated points increases the accuracy of the previously defined camera locations. Therefore, after all referencing was completed; the software again solved and adjusted the camera locations to a more accurate solution.

The process of correlating identification markers was carried out for each of the 15 pressure states. This resulted in a total of 45 total photographs. The Cartesian coordinates of each identification points were extracted from each pressure state. These points were later used as the nodes for the finite element mesh.

3.7 Marker Correlation between Pressure States

Once the 3D points were outputted for each pressure state, each of the markers need to be tracked from one pressure state to the next. This one-to-one correspondence in tracking markers laid the groundwork for the computation of strain in the material. A well-structured array of points allowed for an easy correlation for the rubber membrane. Points were sorted by first x-coordinates and then y-coordinates in each pressure state. Matching the order of points for each pressure states enabled quick and accurate point tracking from one pressure state to the next.

CHAPTER 4 – RESULTS OF A RUBBER MEMBRANE TEST

4.1 Introduction

An in-house finite element method program, FEAP, was modified to output stretch at every node and to complement the stress at every node. Each one of the 15 pressure states were outputted to a data file. This output data was coded in a Tecplot 360® input file. At each node, a both principal stresses were computed along with the Von Mises stress. Principal stretches were also calculated at every pressure state. The Tecplot input file proved a useful way to visually interpret data at every pressure state. Once data files were output for all stretch and stress data it was correlated using Wolfram Mathematica®. Each pressure state was inputted into an array of data. Mathematica was used to organize and compile all data.

4.2 Stress Analysis Results

The geometric features of the membrane, such as smoothness and curvature, greatly influence the quality of stress results. Therefore 3D reconstruction of the mesh determines the value of results. The identification points were more tightly spaced than any successful test previously explored by the research group. At the lowest pressure state the distance between identification points averaged 0.05". The tightness of points accurately captured the surface shape. In previous tests surface smoothing before processing stress results were required (15). This step was omitted due to the accuracy of the reconstruction which automatically rendered a smooth reconstruction of geometric curved surfaces. An example of the reconstruction from photographs is shown in Figure 10.

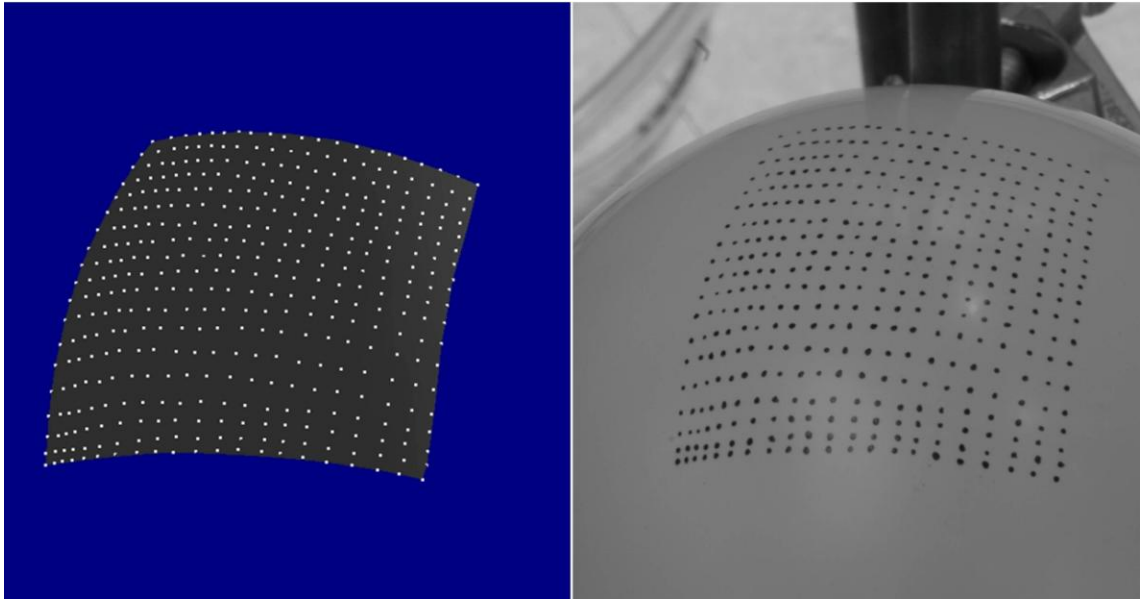


Figure 10. Side-by-Side Comparison of 3D Reconstruction and Actual Photograph.

The stress results were inspected qualitatively. In the photographs, experimental reconstruction error appears as abrupt changes in stress results around a node. One example of this error appears in pressure state 14 of the first principal stresses. This pressure state is shown in Figure 11 and the inaccurate 3D reconstruction is displayed by an abrupt yellow stress increase shown in the middle of the figure.

Minor reconstruction errors appear in only a few pressure states. Overall the stress results appear accurate. Wall stresses range from below 1 lbs/in in the lowest pressure state to over 13 lbs/in in the highest pressure state. A side-by-side comparison of the lowest and highest pressure state is shown in Figure 12. Complete stress plots are shown in Appendix C.

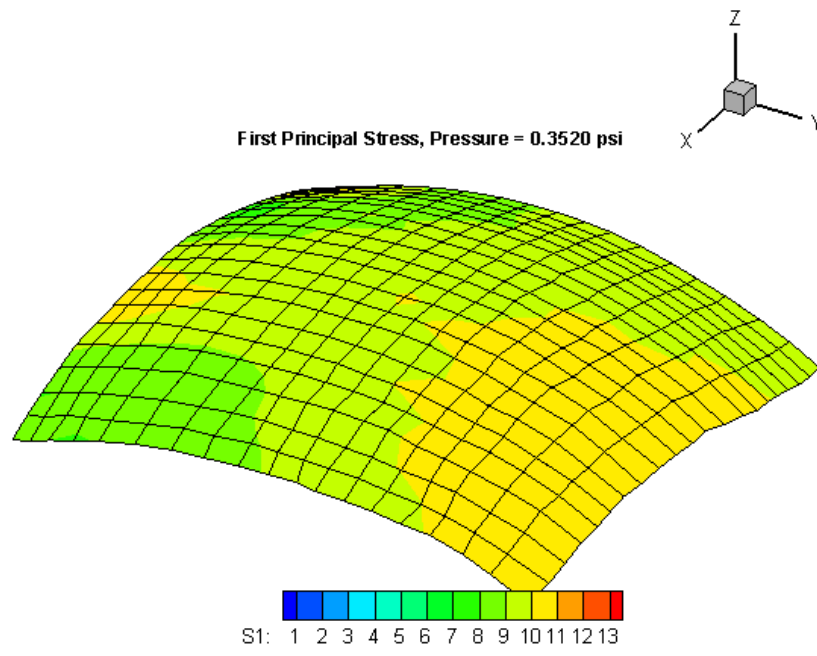


Figure 11. First Principal Stress at Pressure State 14.

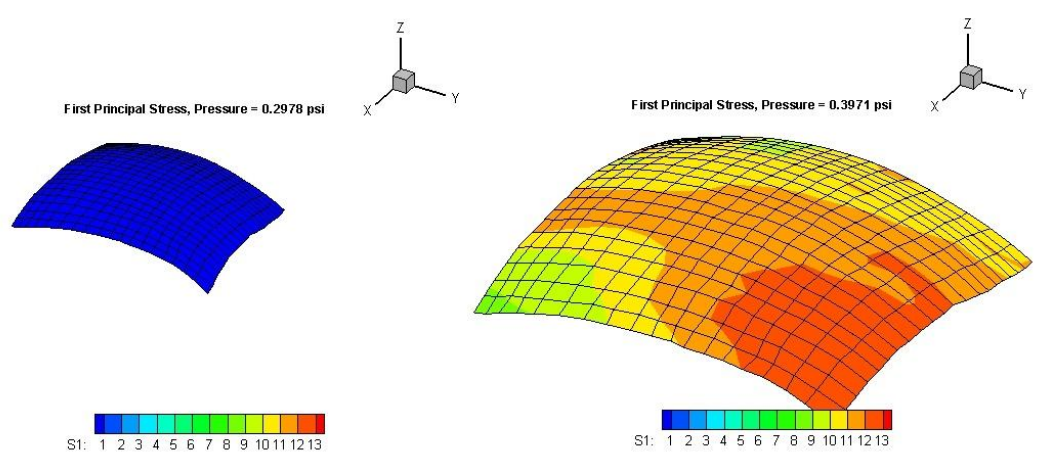


Figure 12. First Principal Stress Results at the lowest and highest pressure state.

4.3 Strain Analysis Results

The stretch data at every membrane point is calculated. A rubber balloon was used for the membrane inflation test. A balloon is usually characterized as a homogeneous material. The data shows a variation in stretch values across the surface; this shows the PWIM was accurate enough to capture heterogeneous properties in a typically assumed homogeneous membrane. It is important to note in a true homogeneous membrane stress and strain results will be uniform across the surface. In the case of the rubber balloon test, variations in stress-strain results were heavily impacted by the slightly non-uniform thickness of the balloon. For example, due to the method used for manufacturing balloons the tip of the balloon has a greater thickness. The thickness material at the tip measured 0.0225 inches with a digital caliper. The rubber membrane's thickness dissipates to approximately 0.0095 inches as the material becomes more uniform away from the tip. The experiment took advantage of this non-uniform thickness by examining an area close to the tip of the balloon to simulate a heterogeneous material.

By examining the first principal stretches at the highest pressure state, shown in Figure 13, the heterogeneous properties became apparent. The lower left corner of Figure 13 shows nodes at the very tip of the balloon, which is the maximum thickness of the membrane. The upper right nodes in Figure 13 are the thinness of the material examined in the membrane. This correlates with expected results due to the thicker material not stretching to the extent of the thinner material. At the deepest shades of red the rubber membrane stretches over 240%. Within the same pressure state there are nodes that show a principal stretch of less than 200%. This 40% difference in material stretching directly shows the PWIM sufficiently delineated a material property map in the membrane.

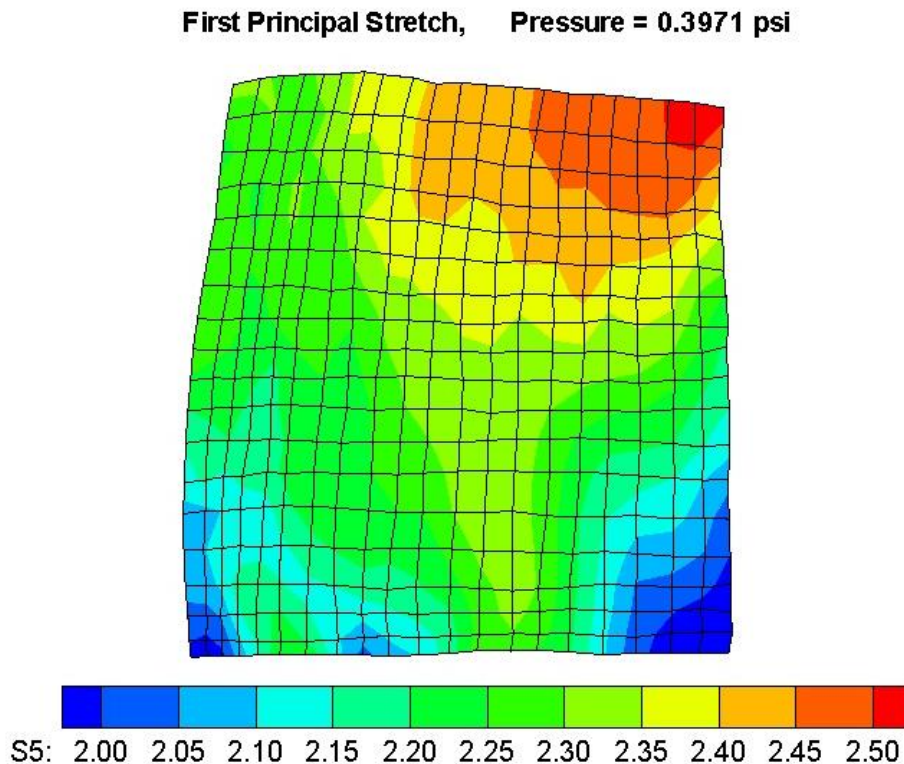


Figure 13. First Principal Stretches at the Highest Pressure State.

4.4 Correlation of Stress-Strain Results

The vast amount of data becomes difficult to interpret when looking through multiple pressure states and different material properties. For example, each material point can be plotted in a 3D coordinate system in different ways. The first node of the mesh can be classified at the first pressure state as an X-value (maximum principal stretch), Y-value (minimum principal stretch), and Z-value (maximum principal stress). The same point can be plotted as a maximum principal stretch, a minimum principal stretch, and the Von Mises stretch at the first node on the first pressure state. To extend the complexity, in the case of the tested membrane there are 15 pressure states and 399 points in every pressure state. This results in almost 6000 discrete points, and with the

abundance in data it is important to extract the extreme areas. The extreme areas are defined as the places on the membrane where the material differs from the rest of the membrane. These areas contain the stiffest material on the membrane or on the other extreme the material that stretches the most.

Combining all pressure state data enables the extraction of the extreme areas. Just as Figure 3 shows the stress versus the elongation of a metal, the derived data shows the principal stresses vs. the principal stretches. All the data in Figure 3 can be captured in a 2D plot, but a heterogeneous nonlinear material is much more complex and the stress and stretch data must be captured by a 3D curve in 3D space. Since each point has a 3D curve, which totaled 399 curves a visual depiction of the material is the best way to convey the information.

For every point, the Von Mises stress was plotted vs. the average principal stretch. The average principal stretch is defined as $(\lambda_1 + \lambda_2)/2$. For each point 15 points exist, one for each pressure state. A logarithmic curve was fit through the 15 points using Mathematica's "FindFit" function. Although this function is a logarithmic curve it can be adapted to any function incorporating any of the variables. To more accurately describe the data the equation could be modified to a different form and incorporate more variables. The format used in the research is,

$$\text{Von Mises Stress} = \alpha \ln\left(\frac{\lambda_1 + \lambda_2}{2}\right) + \beta.$$

The value, α , in this equation represents the value for stiffness. The value of α dictates the steepness of the curve. With a larger the value of α , the stress increases more rapidly for a small change in the stretch. Therefore, this value of α becomes known as the "Stiffness" term.

Each stiffness term was calculated for each of the 399 points. The stiffness terms were correlated with their corresponding node. A Mathworks Matlab program was

completed for complete GUI programming interface. This interface allows the user to explore different nodes and rotate plots to truly grasp a visual understanding of the material properties.

The program starts as a 3D graphical display of the finite element mesh. This quad node mesh was color-coded to the stiffness of the material. For each mesh element the average stiffness was calculated for each of the nodes it contacts. The average value of all four nodes dictates an average stiffness of the element. The maximum and minimum stiffness of elements were calculated. Based on the maximum stiffness and the minimum stiffness each element was colored accordingly. The red elements indicated a maximum stiffness and as the values fade to the minimum, the mesh elements fade to blue. The stiffness mesh is shown in Figure 14. This initial display screen portrays a good starting point for exploring the areas of interest in the membrane more in depth.

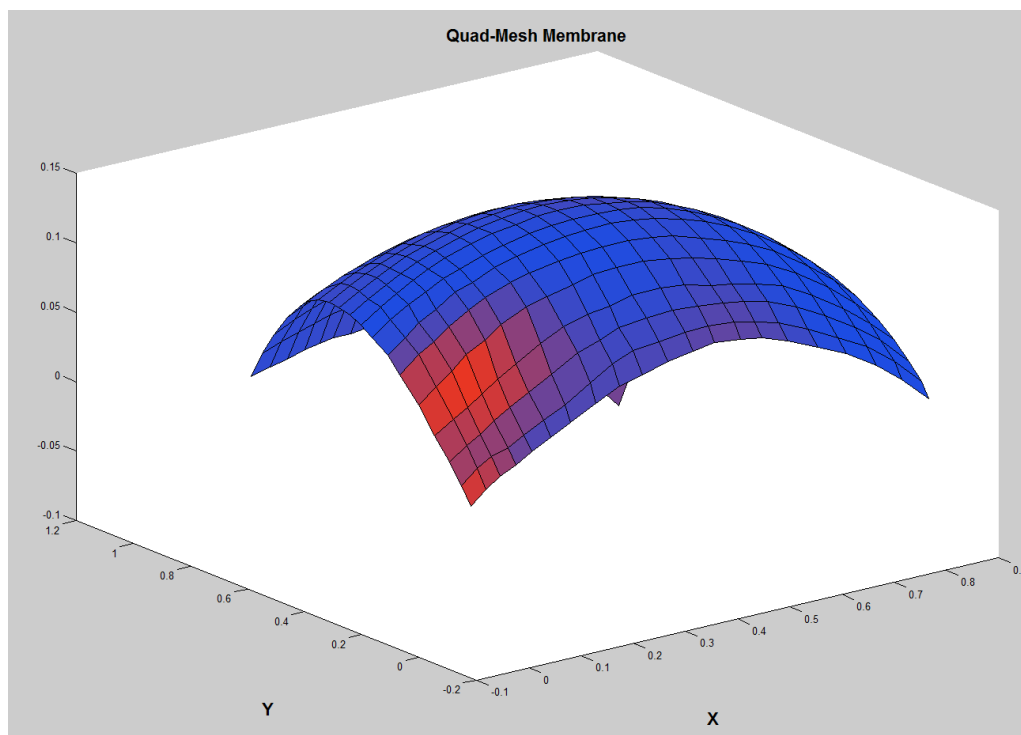


Figure 14. Membrane Mesh showing coloration for stiffness of material.

The program first asks the user to pick a node in the stiffness mesh. After a point is selected, the user proceeds to the graphical results. Three plots are arranged in a full screen mode. The first displays the first principal stress versus the principal stretches, like the sample graph shown in Figure 15. The user has the ability to rotate, pan, and zoom into each plot, making it possible to probe specific pressure states. A sample of the second plot displayed is shown in Figure 16. This plot displays the second principal stress versus the principal stretches. Again, this plot can be probed for specific pressure state values. Lastly, the third plot shows the Von Mises stress versus the average principal stretch, such as the sample shown in Figure 17. Throughout the interactive tool the initially probed node is displayed next to the plot.

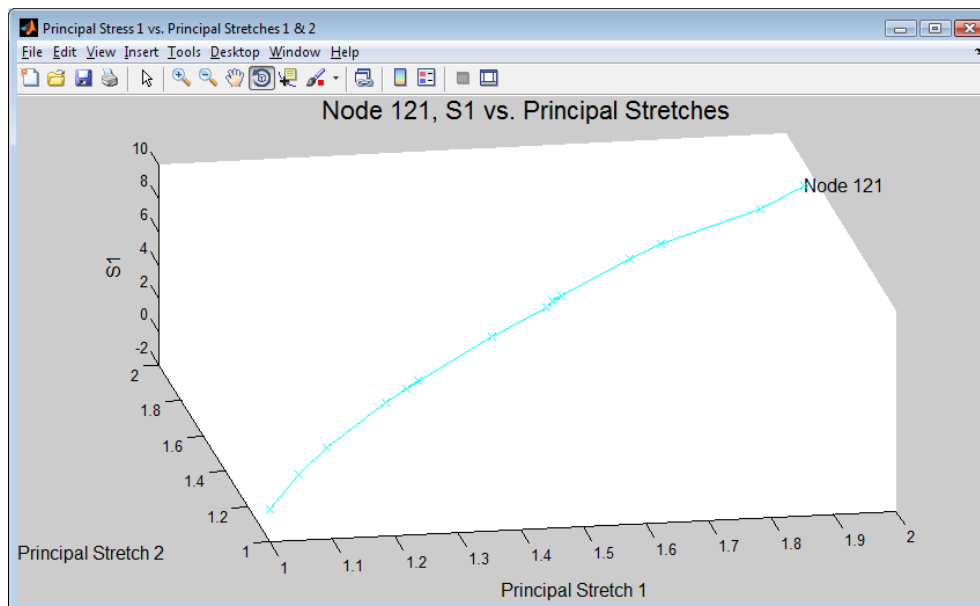


Figure 15. Sample: First Principal Stress vs. Principal Stretches.

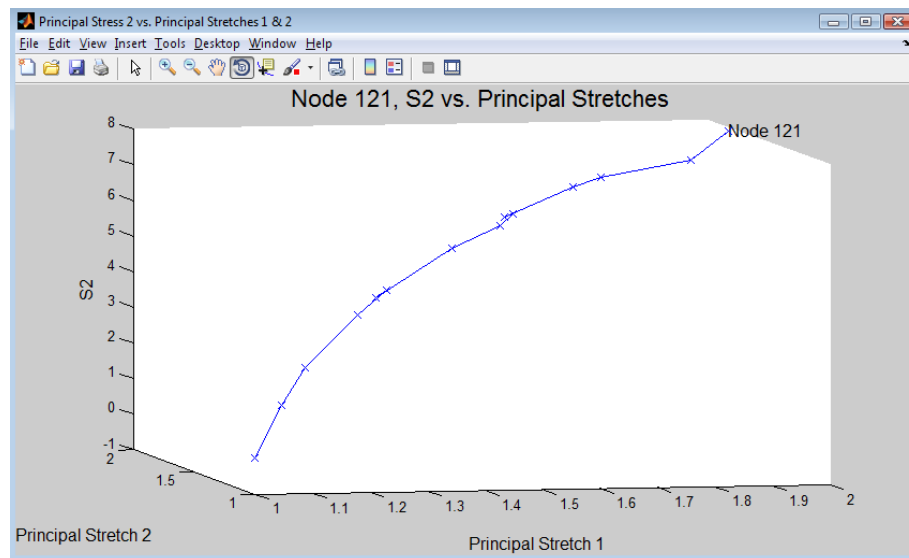


Figure 16. Sample: Second Principal Stress vs. Principal Stretches.

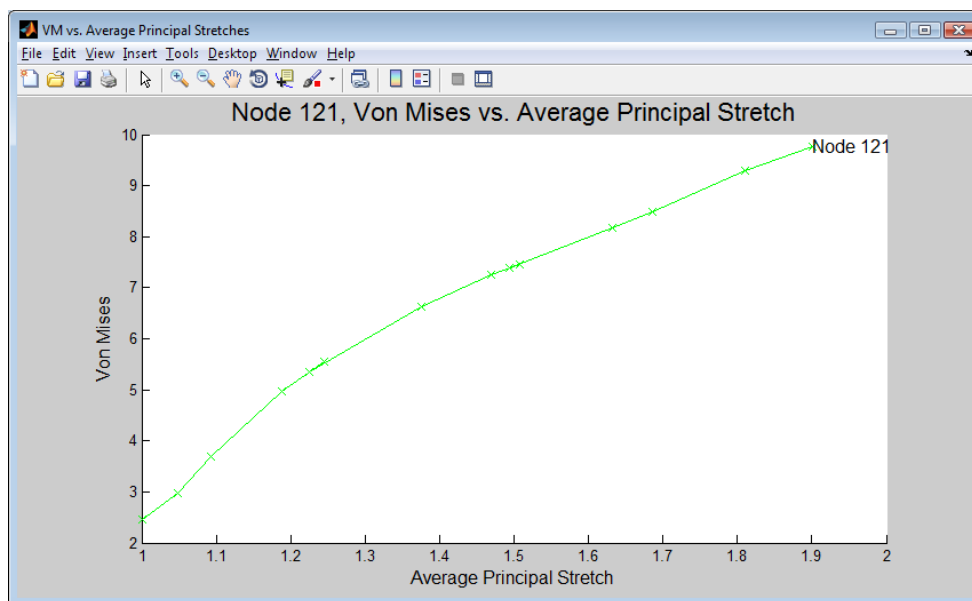


Figure 17. Sample: Von Mises Stress vs. Average Principal Stretch.

The menu allows the user to overlay separate curves from different nodes on top of each other to give the user a comparative tool between nodes. The display plots can either continually be overlaid or the display can be wiped clean. An example of an overlaid plot is shown in Figure 18. When the display is wiped clean new nodes can be compared. Not only does the Matlab interactive mesh provide a good visual tool, it is easily adapted to any heterogeneous mesh. It can be adapted to any number of pressure states and any number of nodes.

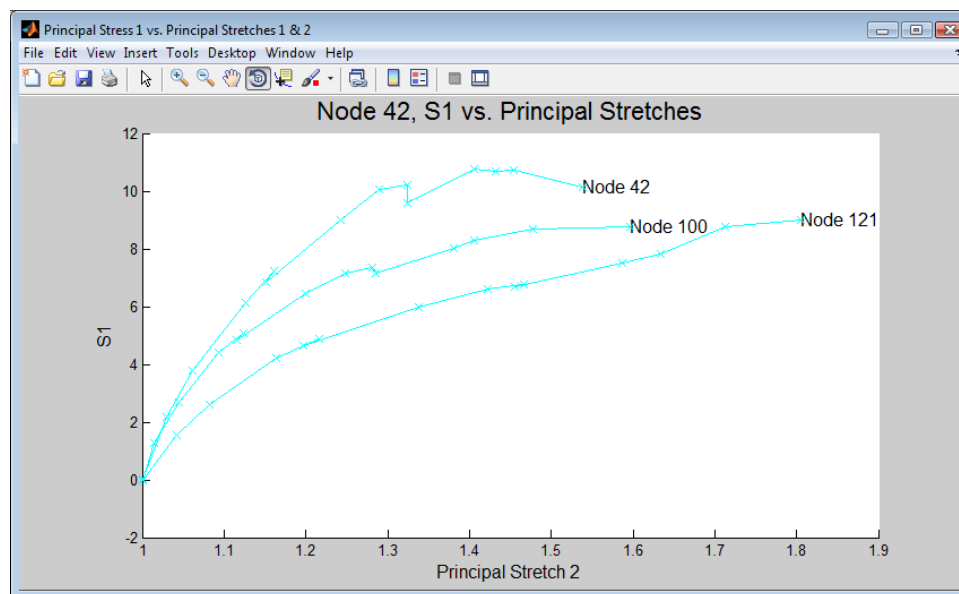


Figure 18. Sample: Overlaid plot of Nodes, Comparing Material Properties

CHAPTER 5 – DISCUSSION OF COMPLEXITIES IN BIOTISSUE TESTING

5.1 Introduction

Many unforeseen problems and complexities exist when preparing the setup for biotissues. During the past years many attempts have been made inflating and testing rabbit bladders. The difficulties range from obtaining bladders to preparing the bladder for testing. A heterogeneous property map of a rabbit bladder is obtainable, but requires advancement in experimental setup and redesign of testing procedures. The following discussion will highlight common problems and explain possible solutions.

5.2 Time Constraints

Bladders were picked up within hours of being harvested from rabbits. The bladders were obtained from a local meat processor, Bud's Custom Meats. The bladders were transported back to the research facility in saline solution. This resulted in approximately an hour before the bladder reaches the research facility. Each bladder remained testable for approximately 48-hours when stored in saline solution on ice. Beyond the 48-hour period, the bladder will harden and becomes brittle. Since processing results can take up to a week, bladders were photographed and disposed of before verifying the photographs captured the markers accurately enough to provide surface reconstruction. A faster and more streamlined process would be desirable.

5.3 Surface Preparation

After the bladders are harvested, fatty tissue remains attached to the surface. This fatty tissue needed to be removed to accurately display the membrane to the camera for smooth surface reconstruction. Although much of the fatty tissue can be removed, a thin mucous film remains around the bladder. This film makes attaching or marking identification points difficult. Drying out the bladder makes marking much easier, but

also destroys the hyperelastic nature of the tissue. Several attempts were made with various types of ink and paint. Both the ink and paint disperses throughout the surface making poor identification points. Instead of ink and paint, a method for marking surfaces with graphite was adapted from Boyce et al (16). The surface was wiped down briefly with alcohol, and graphite flakes were sprinkled on the surface. The dark flakes created a high contrast from the semi-transparent bladder and provided for adequate tracking markers. This method proved to be the most promising for future research. A rabbit bladder marked with graphite flakes is shown in Figure 19. Although graphite flakes provide adequate marking, without a well-ordered marker mesh, tracking points throughout pressure states becomes tedious and time consuming.

Future research could incorporate metal flakes. This method would use an electro-magnetized metal plate to first arrange metal flakes in preferred array. The plate could then be placed against the tissue. Once the plate is in the desired location, the electro-magnet could be disengaged and the metal flakes would fall to their correct locations onto the tissue.

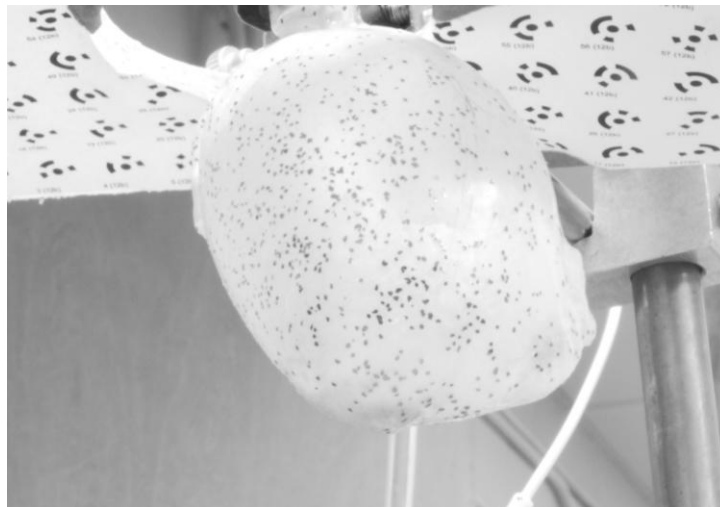


Figure 19. Rabbit Bladder with Graphite Markers.

5.4 Camera Setup

Since the bladder exhibits a wet and shiny surface, camera parameters must be adjusted to compensate. Fluorescent lighting produces glares upon the surface of the bladder concealing the identification markers. All direct lighting was covered with fabric to minimize glare.

The photographs for surface reconstruction require a large depth field to bring all elements into focus. For the large depth needed the camera was adjusted to a very small aperture, acting similar to a pin-hole camera. The small aperture requires a longer exposure time to allow for adequate light to pass through the lens. The long exposure makes the camera susceptible to produce blurry photographs with minuscule movements of the camera. Thus, it is essential to have the camera on a tripod to eliminate movement. A delay timer was placed on the camera to ensure pressing the shutter release button did not producing movement in the photograph.

Once the camera is calibrated for a specific focal length, the camera settings cannot be adjusted. If the camera focal length becomes bumped or slightly adjusted surface reconstruction calculations are ruined. To minimize the potential for this type of human error, tape was placed on the outside of the lens to prohibit any adjustment.

5.5 Inflating the Bladder

To connect the bladder to the air supply, the base of the bladder needs to be clamped to the air tube without air leaks. Sealing the bladder requires an adequate clamping pressure. Clamping the bladder produces a stress concentration around the seal and the bladder often fails when inflated to higher pressure states.

Many times the air pressure will puncture miniature holes in the membrane and result in a loss of pressure. This problem was mitigated by a continuous supply of air into the bladder while holding a steady pressure. However, the leaking air tended to

make the bladder bounce. This poses a problem since it is essential to keep the bladder completely still while taking pictures at various angles to reconstruct the 3D surface.

The bladder also tended to dry out when continually filled with air. This can be countered by continually misting the bladder with saline solution. Problematically, continually misting of the bladder can cause graphite flakes to shift positions. The shifting of graphite flakes anytime during testing will skew points in surface reconstruction and result in unusable data analysis.

Various measures can be taken to improve success of inflating the bladder. A machined fixture for clamping and holding the bladder is essential. Using multiple cameras synced to take pictures simultaneously would also eliminate the bladder shifting positions between exposures. This also would speed up testing therefore the bladder would not need to be misted as often.

CHAPTER 6: CONCLUSION

This experimentation and research was motivated by advancing the technology in capturing material properties of heterogeneous materials. More specifically, this research advanced the PWIM by augmenting an automated surface marker tracking system for measuring the surface strain. The work also qualitatively validated that heterogeneity in membrane property can be revealed using PWIM. The stress and strain computation was decoupled, allowing for quantitative analysis of both stress and strain. The stress computation utilized inverse finite element techniques while applying static determinacy to the convex rubber membrane. The strain computation utilized photogrammetric techniques to track surface markers during inflation of the rubber membrane. This facilitated the quantitative analysis of the stretch at each node of the mesh. Plots were made of both stress and strain data to show a graphical interpretation of the kinematics of the membrane inflation.

The stress and strain data was combined to produce material model curves for 399 locations upon the rubber membrane surface. To further advance usability of material curve data, an interactive software program was made. This tool enables the user to control the point of interest while conducting comparative analysis to other points. The software also allows the user to perceive and interpret vast amounts heterogeneous material property data without being overloaded by large tables of numbers. A material stiffness indicator also can be compared from one point to the next, giving the user knowledge of possible weak areas in the membrane. Thus, this research both validates the PWIM for measuring surface strain, and also provides the research team with an interactive software for future research. In the future, the research can be expanded by devising new ways to improve the surface reconstruction method of the PWIM. These could include faster data acquisition systems with better resolution. This could be done with expanded research in image processing and more advanced 3D scanning devices.

Lastly, the research expands on the difficulties of testing biological tissues. This discussion provides a guide for future research to optimize preparation and testing techniques.

REFERENCES

1. *Elasticity of Soft Tissues in Simple Elongation*. **Fung, Y.C.B.** 6, December 6, 1967, American Journal of Physiology, Vol. 213, pp. 1532-1544.
2. *Mechanical Stresses in Abdominal Aortic Aneurysms: Influence of Diameter, Asymmetry, and Material Anisotropy*. **Rodriguez, Jose F., Ruiz, Cristina and Doblare, Manuel.** [ed.] Gerhard A. Holzappel. s.l. : ASME, April 2008, Journal of Biomechanical Engineering, Vol. 130.
3. *Transverse Stiffness: A Method for Estimation of Myocardial Wall Stress*. **Halperin, H.R., et al.** s.l. : American Heart Association, 1987, Journal of the American Heart Association, Vol. 61, pp. 695-703.
4. *Tensile Properties of Human Knee Joint Cartilage: I. Influence of Ionic Conditions, Weight Bearing, and Fibrillation on the Tensile Modulus*. **Akizuki, Shaw, et al.** s.l. : Raven Press, 1986, Journal of Orthopaedic Research, Vol. 4, pp. 379-392.
5. *Inverse method of stress analysis for cerebral aneurysms*. **Lu, Jia, Zhou, Xianlian and Raghavan, Madhavan.** 6, December 1, 2008, Biomechanics and Modeling in Mechanobiology, Vol. 7, pp. 477-486.
6. *Pointwise Identification of Elastic Properties in Nonlinear Hyperelastic Membranes - Part I: Theoretical and Computational Developments*. **Lu, Jia and Zhao, Xuefeng.** November 2009, ASME Journal of Applied Mechanics, Vol. 76, pp. 061013/1-061013-10.
7. *A Triplane Video-Based Experimental System for Studying Axisymmetrically Inflated Biomembranes*. **Hsu, Frank P.K., et al.** 5, May 1995, IEEE Transactions on Biomedical Engineering, Vol. 42, pp. 442-450.
8. **Mase, G. Thomas, Smelser, Ronald E. and Mase, George E.** *Continuum Mechanics for Engineers*. 3rd Edition. Boca Raton : CRC Press, 2010. pp. 285-292.
9. *Torsion of a Rubber Cylinder*. **Rivlin, R.S.** 5, s.l. : American Institute of Physics, May 1947, Journal of Applied Physics, Vol. 18, pp. 444-449.
10. *Characterization of Hyperelastic Rubber-like materials by Biaxial and Uniaxial Stretching Tests based on Optical Methods*. **Sasso, M., Palmieri, G. and Chiappini, D. Amodio.** 2008, Polymer Testing, Vol. 27, pp. 995-1004.
11. **Naghdi, P.M.** *Notes on Continuum Mechanics*. Department of Mechanical Engineering, University of California at Berkeley. 2001. pp. 1-44.
12. *Computational Methods for Inverse Deformation in Quasi-Incompressible Finite Elasticity*. **Govindjee, Sanjay and Mihalic, Paul A.** 5, 1998, International Journal for Numerical Methods in Engineering, Vol. 43, pp. 821-838.
13. *Inverse Formulation for Geometrically Exact Stress Resultant Shells*. **Zhou, Xianlian and Lu, Jia.** 2008, International Journal for Numerical Methods in Engineering, Vol. 74, pp. 1278-1302.

14. **Luhmann, Thomas, et al.** *Close Range Photogrammetry: Principles, Methods and Applications*. s.l. : Whittles Publishing, 2006. ISBN 0-470-10633-6.
15. **Zhao, Xuefeng.** *Pointwise Identification of Elastic Properties in Nonlinear Heterogeneous Membranes, and Application to Soft Tissues*. Department of Mechanical Engineering, University of Iowa. Iowa City : s.n., 2009.
16. *Full-field deformation of bovine cornea under constrained inflation conditions.*
Boyce, Brad L., et al. 28, October 2008, *Biomaterials*, Vol. 29, pp. 3896-3904.

APPENDIX A – MATHEMATICA CODE

This data transforms the individual pressure state output files from a Tecplot data file into a spreadsheet data files. After spreadsheet data is created, the code then calculates the stiffness of each of the nodes based on heterogeneous stretch data at each node throughout all pressure states.

```

Clear[a]
Clear[S1,i,j];
Clear[S2,VM,PrincStretch1,PrincStretch2]
Clear[Data];
NumberOfPressureStates=15;

CXLocation=1;
CYLocation=2;
CZLocation=3;
XLocation=4;
YLocation=5;
ZLocation=6;
ULocation=7;
VLocation=8;
WLocation=9;
S1Location=10;
S2Location=11;
S3Location=12;
ShearLocation=13;

```

PrincStretch1Location=14;

PrincStretch2Location=15;

P1Location=16;

P2Location=17;

P3Location=18;

Data1=Import["H:\\feapcode/TP_Ip01_1.0000.dat", "Table"];

Data2=Import["H:\\feapcode/TP_Ip02_1.0000.dat", "Table"];

Data3=Import["H:\\feapcode/TP_Ip03_1.0000.dat", "Table"];

Data4=Import["H:\\feapcode/TP_Ip04_1.0000.dat", "Table"];

Data5=Import["H:\\feapcode/TP_Ip05_1.0000.dat", "Table"];

Data6=Import["H:\\feapcode/TP_Ip06_1.0000.dat", "Table"];

Data7=Import["H:\\feapcode/TP_Ip07_1.0000.dat", "Table"];

Data8=Import["H:\\feapcode/TP_Ip08_1.0000.dat", "Table"];

Data9=Import["H:\\feapcode/TP_Ip09_1.0000.dat", "Table"];

Data10=Import["H:\\feapcode/TP_Ip10_1.0000.dat", "Table"];

Data11=Import["H:\\feapcode/TP_Ip11_1.0000.dat", "Table"];

Data12=Import["H:\\feapcode/TP_Ip12_1.0000.dat", "Table"];

Data13=Import["H:\\feapcode/TP_Ip13_1.0000.dat", "Table"];

Data14=Import["H:\\feapcode/TP_Ip14_1.0000.dat", "Table"];

Data15=Import["H:\\feapcode/TP_Ip15_1.0000.dat", "Table"];

Data={Data1,Data2,Data3,Data4,Data4,Data5,Data6,Data7,Data8,Data9,Data10,Data11,
Data12,Data13,Data14,Data15};

NumberOfNodes=Data[[1]][[3,5]];

Coordinates=Array[0&,{NumberOfNodes,3}];

```

For[i=1,i<= NumberOfNodes,i++,
For[j=1,j<=3,j++,
Coordinates[[i,j]=Data[[1]][[i+4,j]]]
GetVariableData[VariableName_,Column_]:=
Module[{ },VariableName=Array[0&,{NumberOfNodes,NumberOfPressureStates}];
For[i=1,i<= NumberOfNodes,i++,
For[j=1,j<=NumberOfPressureStates,j++,
VariableName[[i,j]=Data[[j]][[i+4,Column]]]]]
GetVariableData[S1,S1Location];
GetVariableData[S2,S2Location];
GetVariableData[PrincStretch1,PrincStretch1Location];
GetVariableData[PrincStretch2,PrincStretch2Location];

VM=Sqrt[((S1-S2)^2+S1^2+S2^2)/2];
ExportData={Coordinates,S1,S2,VM,PrincStretch1,PrincStretch2};
Export["H:\\feapcode/StretchData.xls",ExportData,{"Data"}];
Export["H:\\feapcode/Coordinates.csv",Coordinates,{"Data"}];
Export["H:\\feapcode/S1.csv",S1,{"Data"}];
Export["H:\\feapcode/S2.csv",S2,{"Data"}];
Export["H:\\feapcode/VM.csv",VM,{"Data"}];
Export["H:\\feapcode/PrincipalStretch1.csv",PrincStretch1,{"Data"}];
Export["H:\\feapcode/PrincipalStretch2.csv",PrincStretch2,{"Data"}];
Stiffness=Array[0&,NumberOfNodes];
CalculatePointStiffness[PointNumber_]:=
Module[{ },

```

```

Data=Array[0&,{NumberOfPressureStates,2}];
For[i=1,i<=NumberOfPressureStates,i++,
Data[[i,1]]=(PrincStretch1[[PointNumber,i]]+PrincStretch2[[PointNumber,i]])/2;
Data[[i,2]]=VM[[PointNumber,i];
]
]
bvals=Array[0&,NumberOfNodes];
For[j=1,j<=NumberOfNodes,j++,
Clear[a,b,sol,x];
CalculatePointStiffness[j];
sol=FindFit[Data,a Log[x]+b,{a,b},x][[1]];
sol1=FindFit[Data,a Log[x]+b,{a,b},x][[2]];
Stiffness[[j]]=a/.sol;
bvals [[j]]=b/.sol1;
]

d=Mean[bvals];

For[j=1,j<=NumberOfNodes,j++,
Clear[a,b,sol,x];
CalculatePointStiffness[j];
sol=FindFit[Data,a Log[x]+d,{a},x][[1]];
Stiffness[[j]]=N[a/.sol,5];
]

Export["H:\\feapcode/Stiffness.csv",Stiffness,{"Data"}];

```

APPENDIX B – MATLAB CODE

This Matlab code reads from the previous spreadsheet files output by the Mathematica code and generates a GUI interface to explore heterogeneous properties at each node.

```

clf reset

coordinates = csvread('Coordinates.csv');
loop=1;
cancel=0;

while (loop==1)

%%%%%%%%%%%%Plot Nodes

NumberOfNodes=size(coordinates,1);
nodesxy=[coordinates(:,1) coordinates(:,2)];
ElementNodes=csvread('ElementShape.csv');
NumberOfElements=size(ElementNodes,1);
Stiffness=csvread('Stiffness.csv');

quad_surface_display ( NumberOfNodes, transpose(nodesxy),
NumberOfElements, transpose(ElementNodes),
coordinates(:,3),Stiffness);

%%%%%%%%%%%%Pick Node and Press Enter

datacursormode on

dcmObj = datacursormode(figure(1));

```



```

scrsz = get(0,'ScreenSize');
set (figure(1),'Position',[175 1 scrsz(3)-175 scrsz(4)-75])
set(figure(1),'Name','Nodes','NumberTitle','off')

```

```

choicel = menu('Pick A Point','Enter','Enter Node Number');

```

```

switch choicel

```

```

    case 1

```

```

        point1=getCursorInfo(dcmObj);

```

```

        x = point1.Position(1);

```

```

        y = point1.Position(2);

```

```

        z = point1.Position(3);

```

```

        %%%%%%%%%Find which Node is Picked

```

```

            i=1;

```

```

            while (x~=coordinates(i,1))

```

```

                i=i+1;

```

```

            end

```

```

    case 2

```

```

        prompt={'Node Number'}

```

```

        defans={'1'}

```

```

        fields = {'num'}

```

```

        info = inputdlg(prompt, 'Enter Node Number', 1,
defans)

```

```

        if ~isempty(info)                                %see if user hit
cancel
        info = cell2struct(info,fields)

        datanodenummer = str2num(info.num)    %convert
string to number

        i=datanodenummer;

        else

            cancel=1;

        end

end

end

if cancel==1

    close all

    return

end

%%%%%%%%%%%%Import Data for picked node

%CSV File starts at position '0' so back up counter

i=i-1;

S1 = csvread('S1.csv',i,0,[i,0,i,14]);

S2=csvread('S2.csv',i,0,[i,0,i,14]);

VM=csvread('VM.csv',i,0,[i,0,i,14]);

PrincStr1=csvread('PrincipalStretch1.csv',i,0,[i,0,i,14]);

PrincStr2=csvread('PrincipalStretch2.csv',i,0,[i,0,i,14]);

```

```

%%%%%%%%%%%%%%%%%%%%%%%%%%%%%%%%%%%%%%%%%%%%%%%%%%%%%%%%%%%%%%%%%%%%%%%%Plot Data

%Redisplay Figure 1

figure(1)

set (figure(1),'Position',[1 scrsz(4)/2+12 scrsz(3)/2
scrsz(4)/2-87])

%S1-Upper Right

figure(2)

set(figure(2),'Position',[scrsz(3)/2 scrsz(4)/2+12
scrsz(3)/2 scrsz(4)/2-87])

set(figure(2),'Name','Principal Stress 1 vs. Principal
Stretches 1 & 2','NumberTitle','off')

hold on;

plot3(PrincStr1,PrincStr2,S1,'-xc','markersize', 8)

xlabel('Principal Stretch 1','FontSize',12)

ylabel('Principal Stretch 2','FontSize',12)

zlabel('S1','FontSize',12)

title(sprintf('Node %i, S1 vs. Principal Stretches',
(i+1)), 'FontSize',16)

text(PrincStr1(1,15),PrincStr2(1,15),S1(1,15),sprintf('Node
%i', (i+1)), 'FontSize',12)

view([1,0,0])

%S2-Lower Left

figure(3)

set(figure(3),'Position',[1 25 scrsz(3)/2 scrsz(4)/2-87])

```

```

set(figure(3),'Name','Principal Stress 2 vs. Principal
Stretches 1 & 2','NumberTitle','off')

hold on;

plot3(PrincStr1,PrincStr2,S2,'-xb','markersize', 8)

hold on;

xlabel('Principal Stretch 1','FontSize',12)
ylabel('Principal Stretch 2','FontSize',12)
zlabel('S2','FontSize',12)

title(sprintf('Node %i, S2 vs. Principal Stretches',
(i+1)),'FontSize',16)

text(PrincStr1(1,15),PrincStr2(1,15),S2(1,15),sprintf('Node
%i', (i+1)),'FontSize',12)

view([0,-1,0])

%VM-LowerRight

figure(4)

set(figure(4),'Position',[scrsz(3)/2 25 scrsz(3)/2
scrsz(4)/2-87])

set(figure(4),'Name','VM vs. Average Principal
Stretches','NumberTitle','off')

hold on;

plot(((PrincStr1+PrincStr2)/2),VM,'-xg','markersize', 8)

xlabel('Average Principal Stretch','FontSize',12)

ylabel('Von Mises','FontSize',12)

title(sprintf('Node %i, Von Mises vs. Average Principal
Stretch', (i+1)),'FontSize',16)

text((PrincStr1(1,15)+PrincStr2(1,15))/2,VM(1,15),sprintf('
Node %i', (i+1)),'FontSize',12)

```

```
choice = menu('Enter Selection','Examine a New  
Point','Clear Screen','Quit');  
  
switch choice  
    case 1  
        loop=1;  
    case 2  
        clf(figure(2),'reset')  
        clf(figure(3),'reset')  
        clf(figure(4),'reset')  
    case 3  
        loop=0;  
  
end  
  
end  
  
close all;
```

Published with MATLAB® 7.8

APPENDIX C – TECPLOT STRESS RESULTS

The following plots show stress distributions at all pressure states.

C.1 First Principal Stresses of Rubber Membrane Test

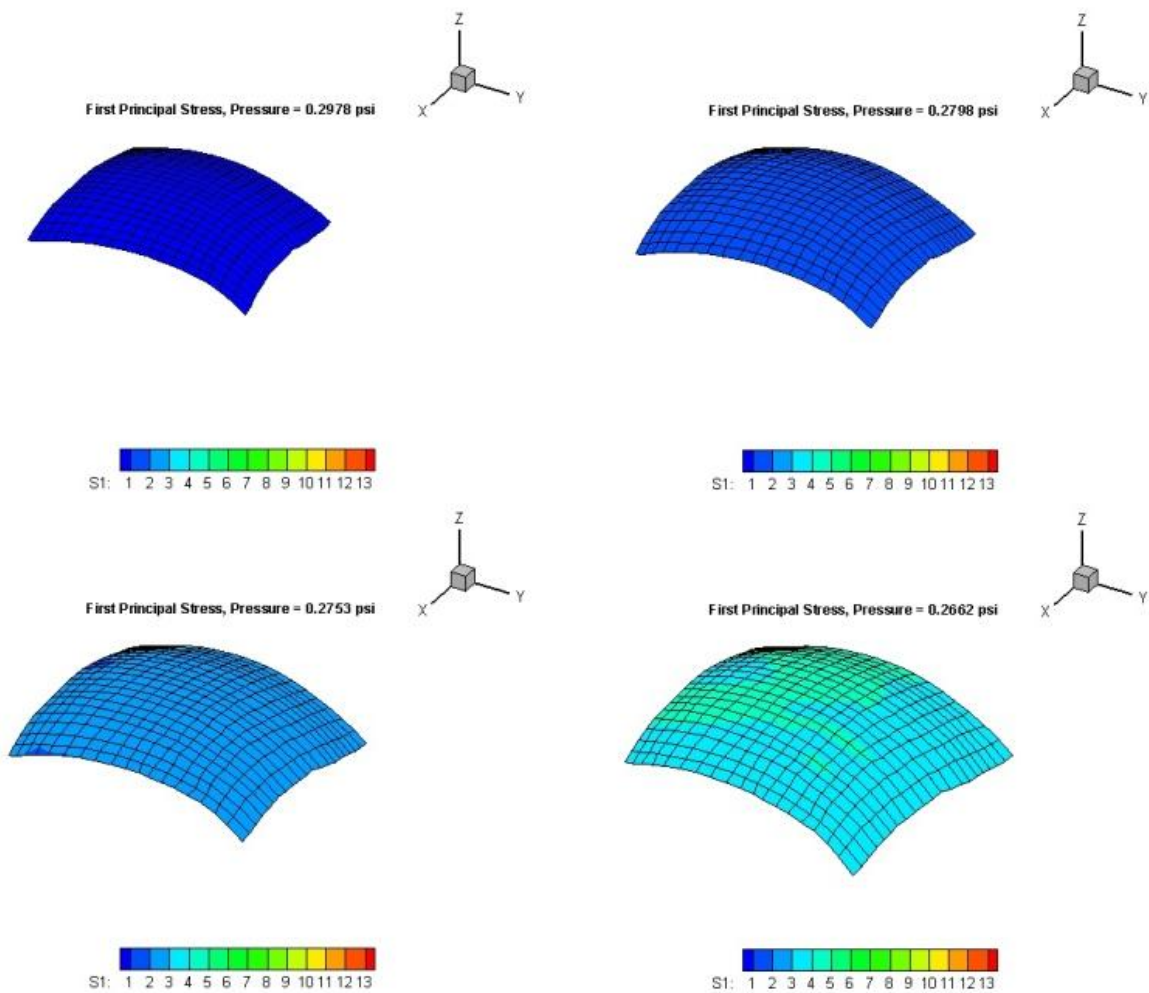


Figure C1. First Principal Stresses, Pressure States 1 through 4.

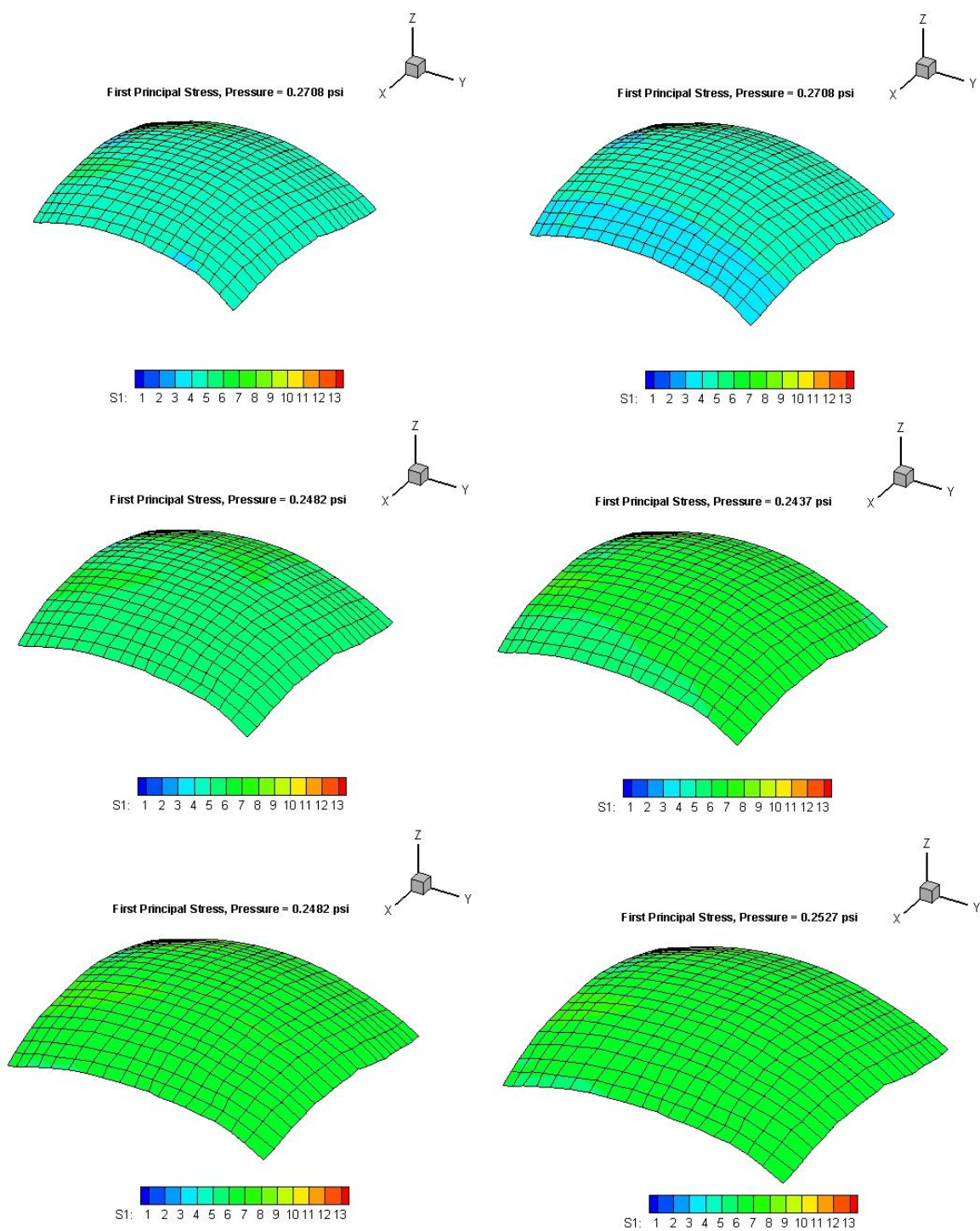


Figure C2. First Principal Stresses, Pressure States 5 through 10.

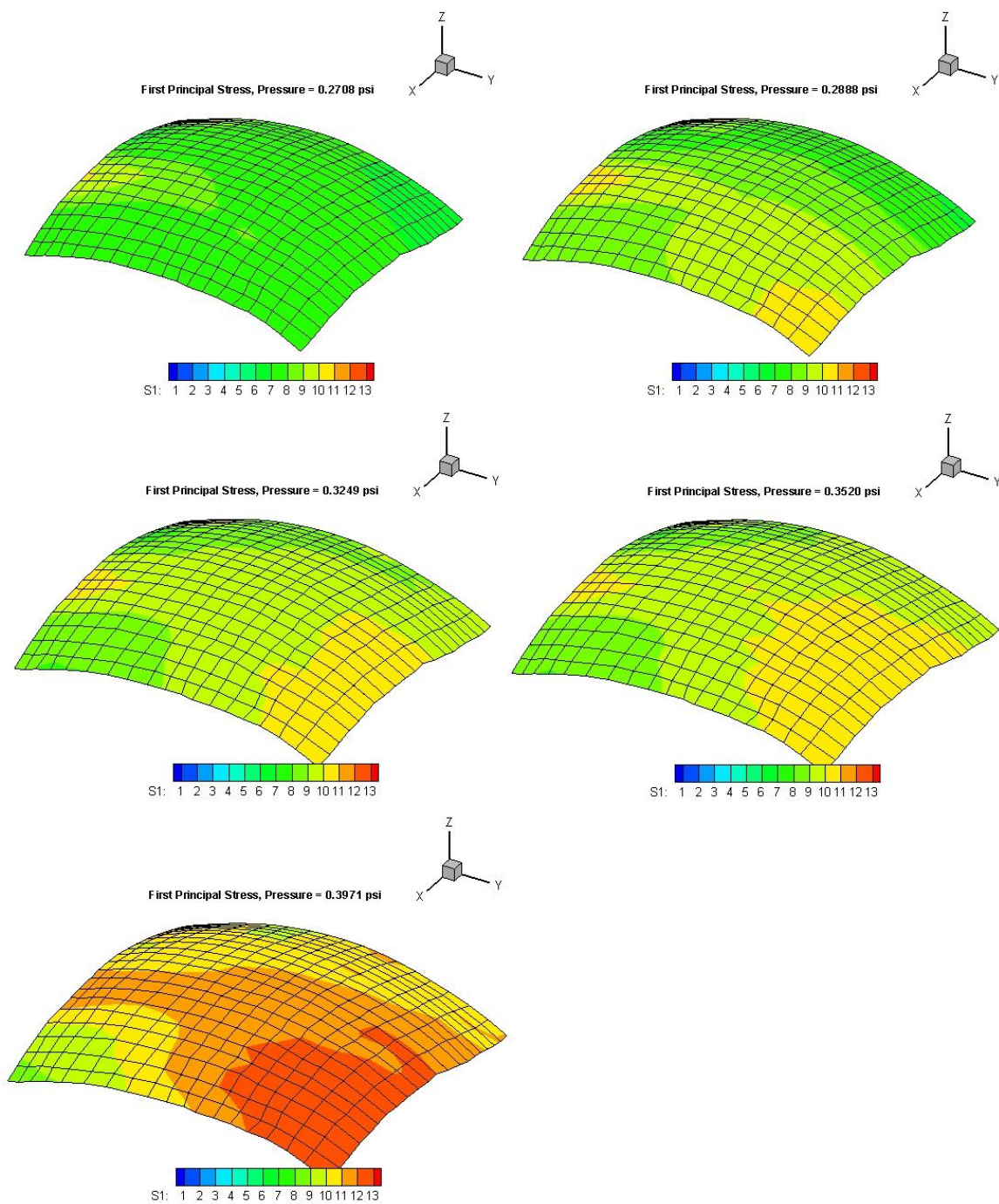


Figure C3. First Principal Stresses, Pressure States 11 through 15.

C.2 Second Principal Stresses of Rubber Membrane Test

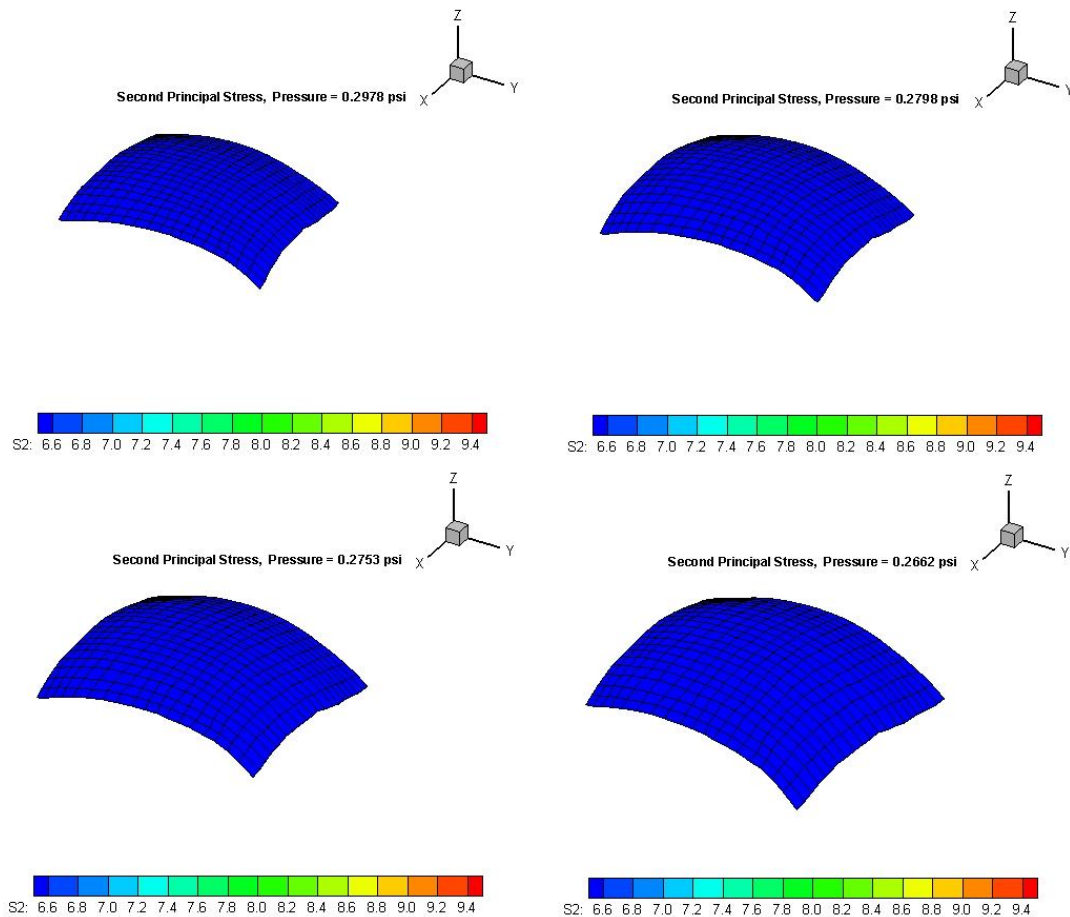


Figure C4. Second Principal Stresses, Pressure States 1 through 4.

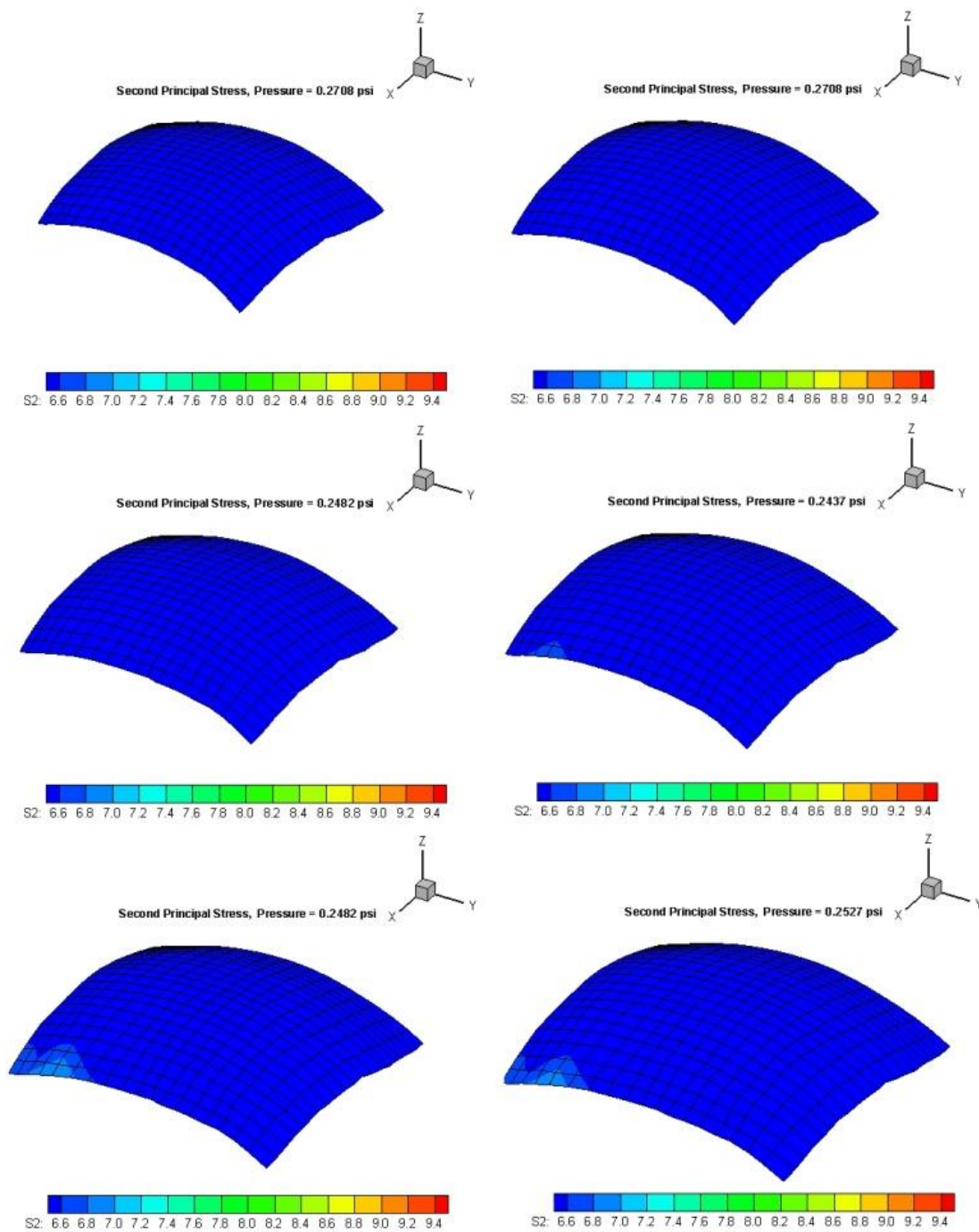


Figure C5. Second Principal Stresses, Pressure States 5 through 10.

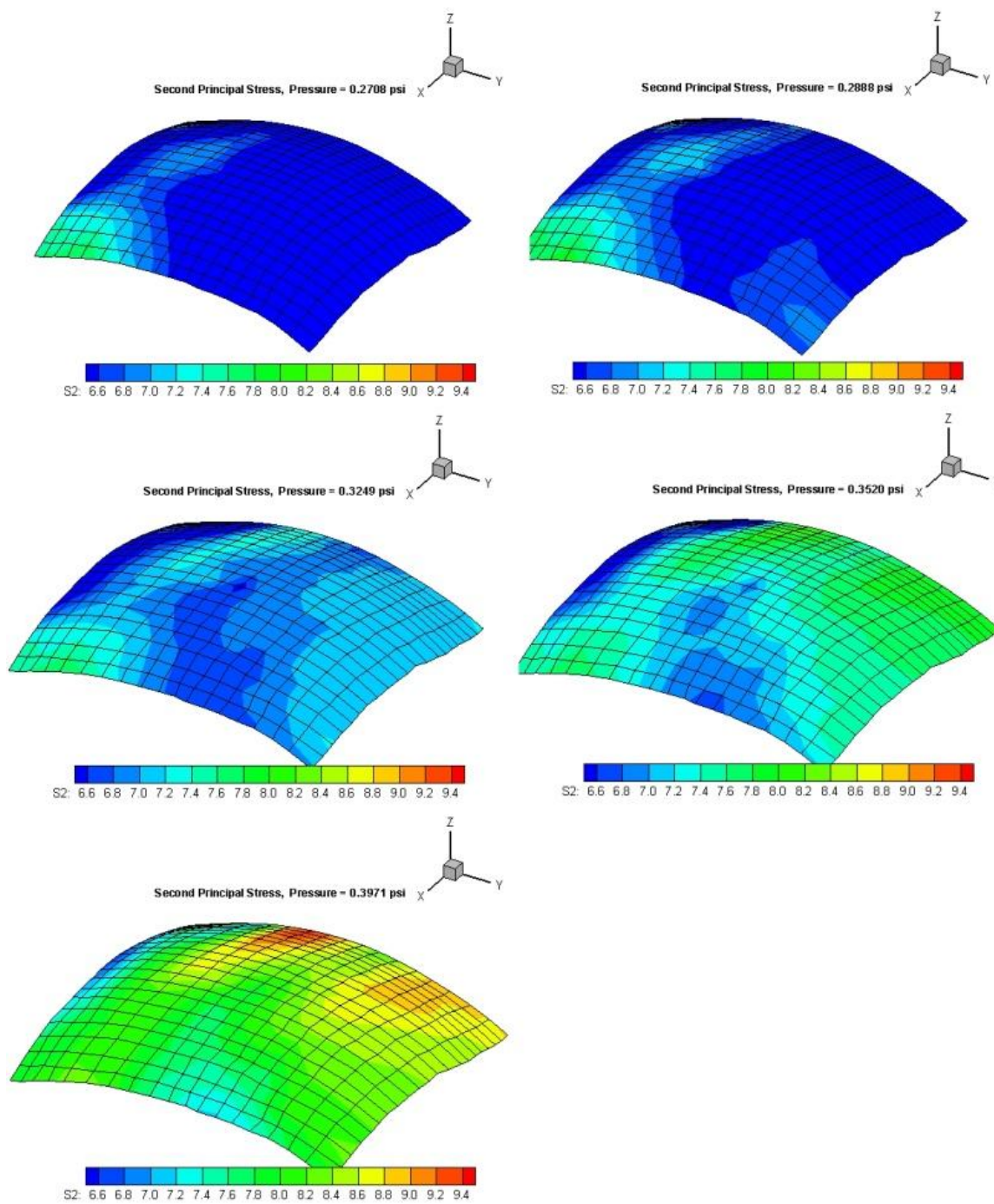


Figure C6. Second Principal Stresses, Pressure States 11 through 15.

APPENDIX D – TECPLOT STRETCH RESULTS

The following plots show stretch (strain) distributions at all pressure states.

D.1 First Principal Stretches of Rubber Membrane Test

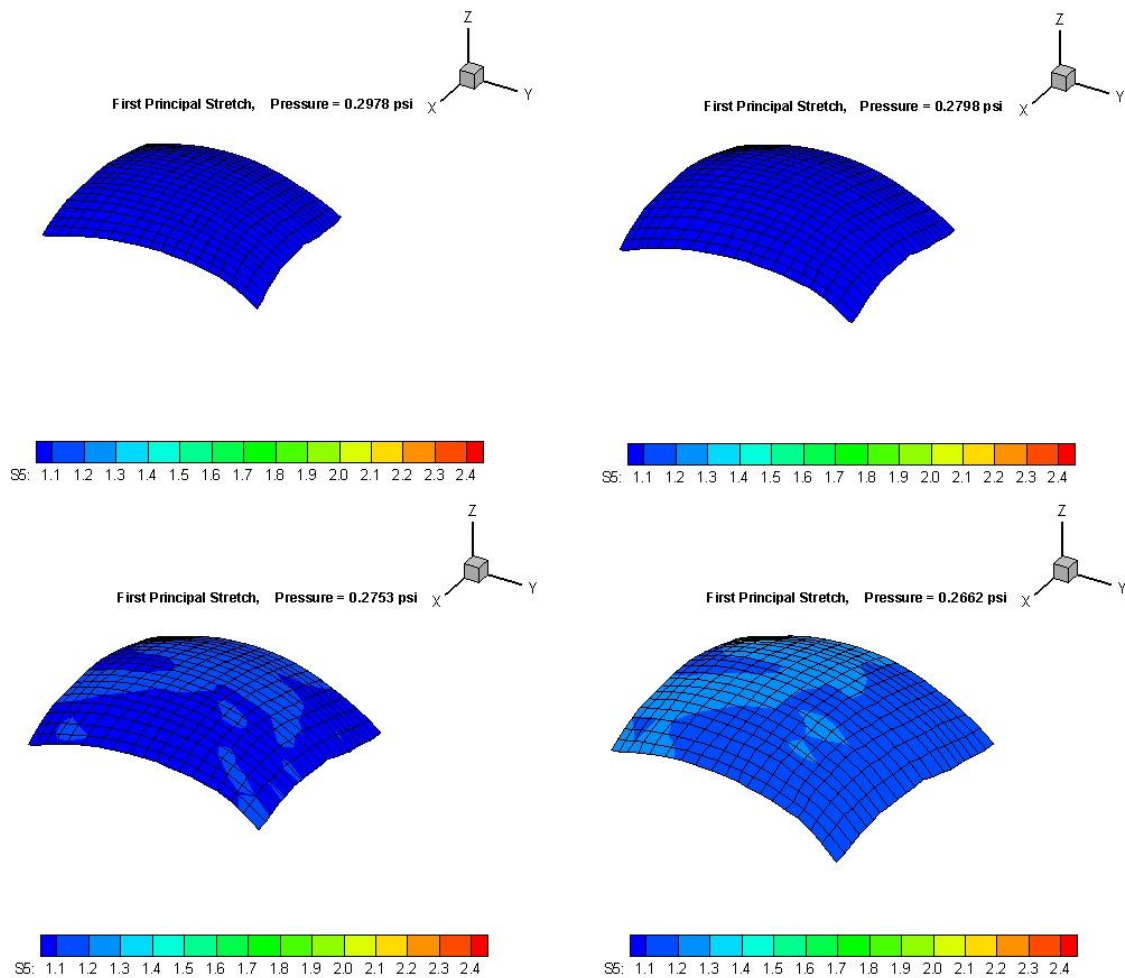


Figure D1. First Principal Stretches, Pressure States 1 through 4.

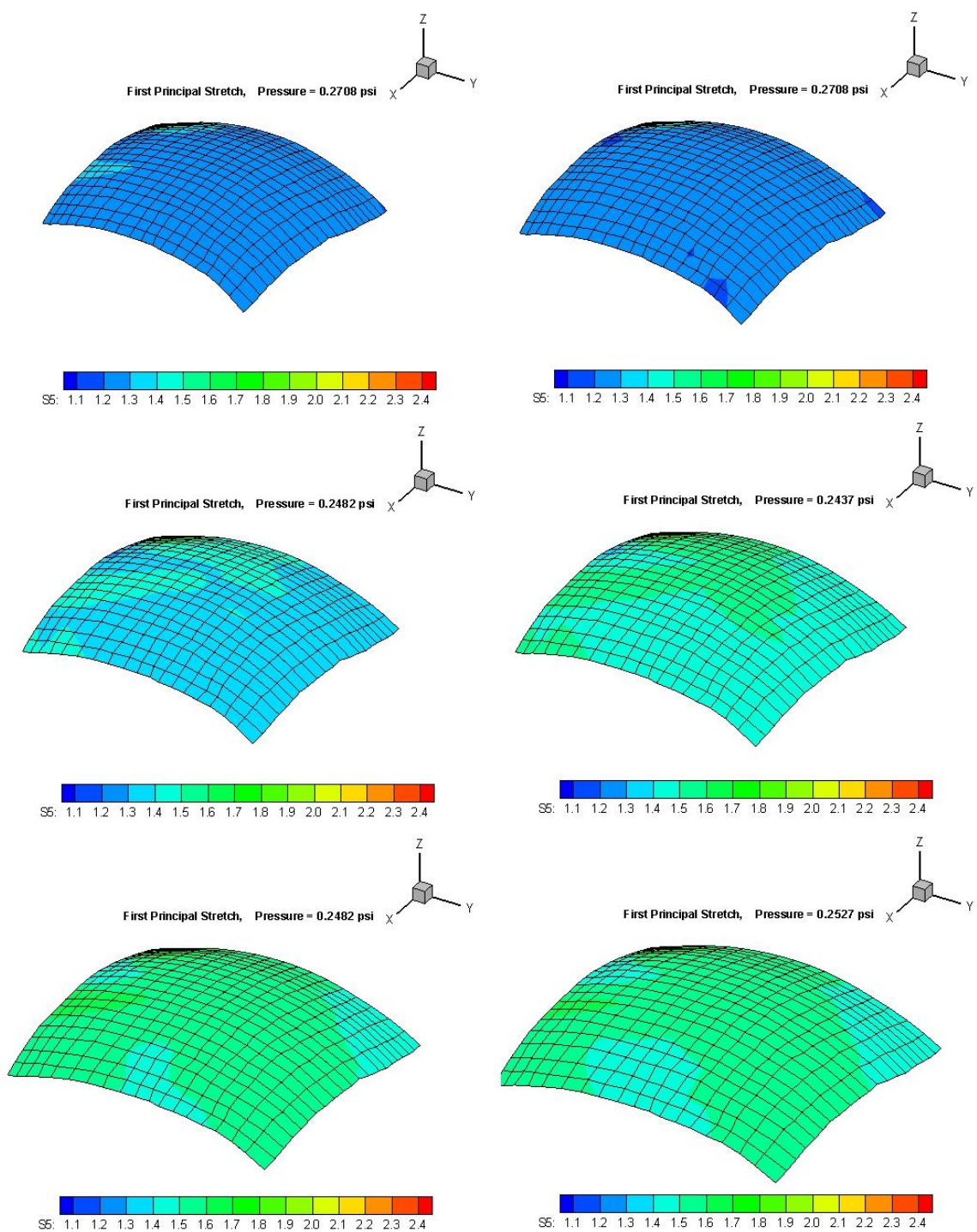


Figure D2. First Principal Stretches, Pressure States 5 through 10.

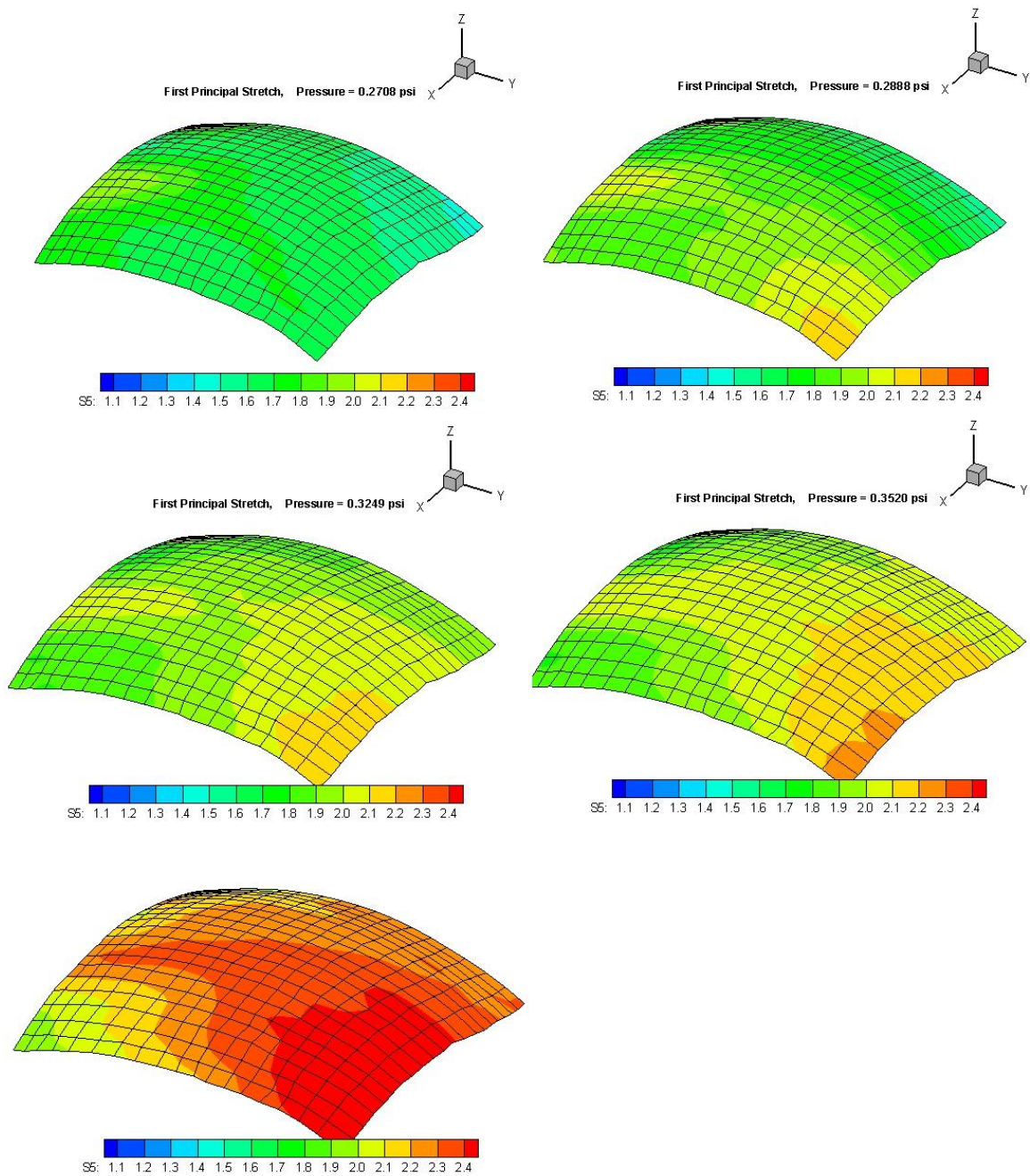


Figure D3. First Principal Stretches, Pressure States 11 through 15.

D.2 Second Principal Stretches of Rubber Membrane Test

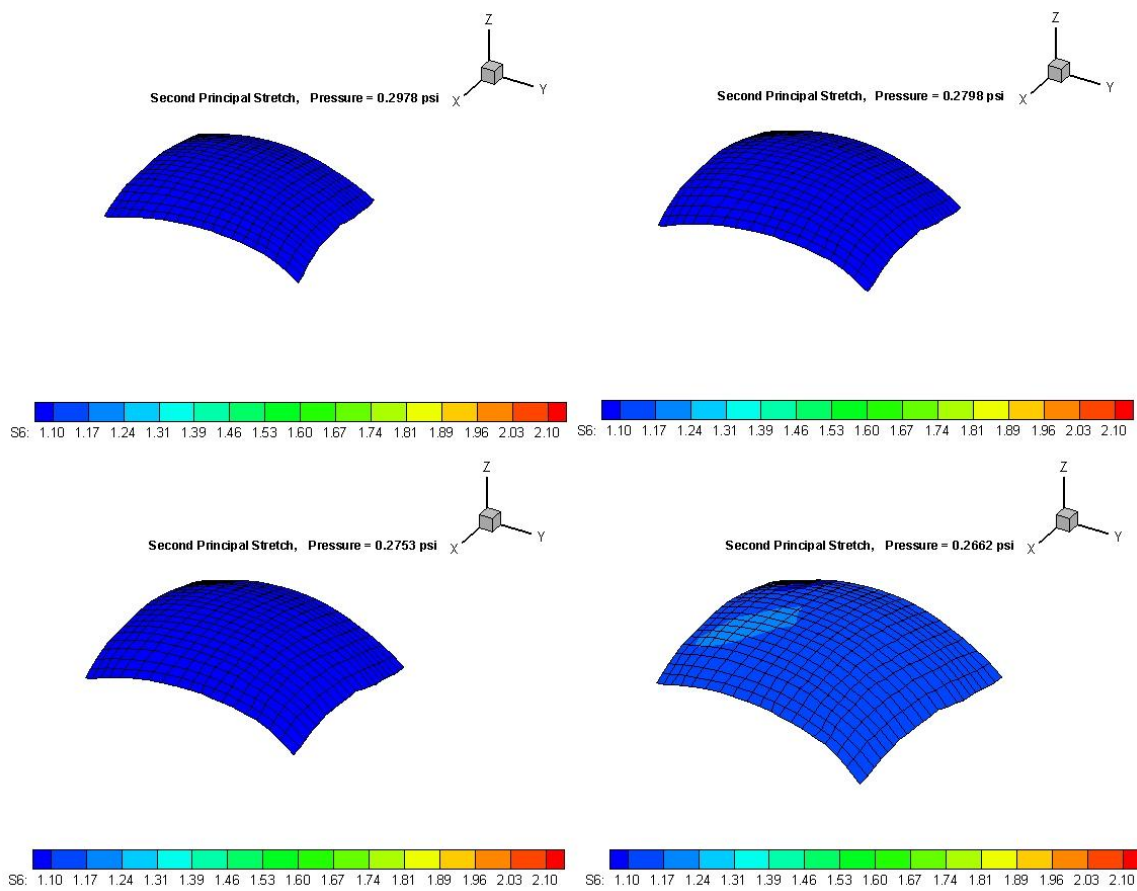


Figure D4. Second Principal Stretches, Pressure States 1 through 4.

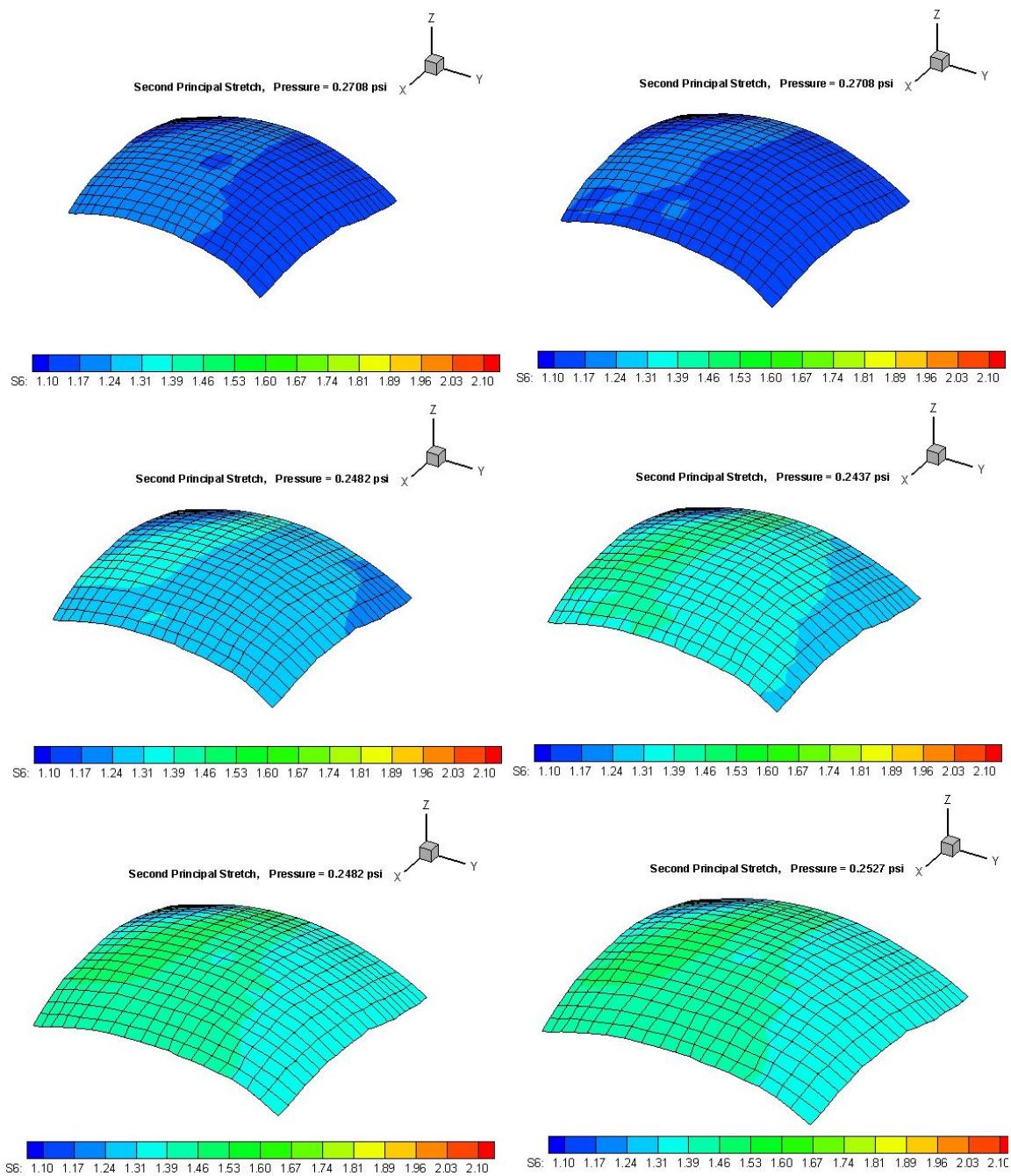


Figure D5. Second Principal Stretches, Pressure States 5 through 10.

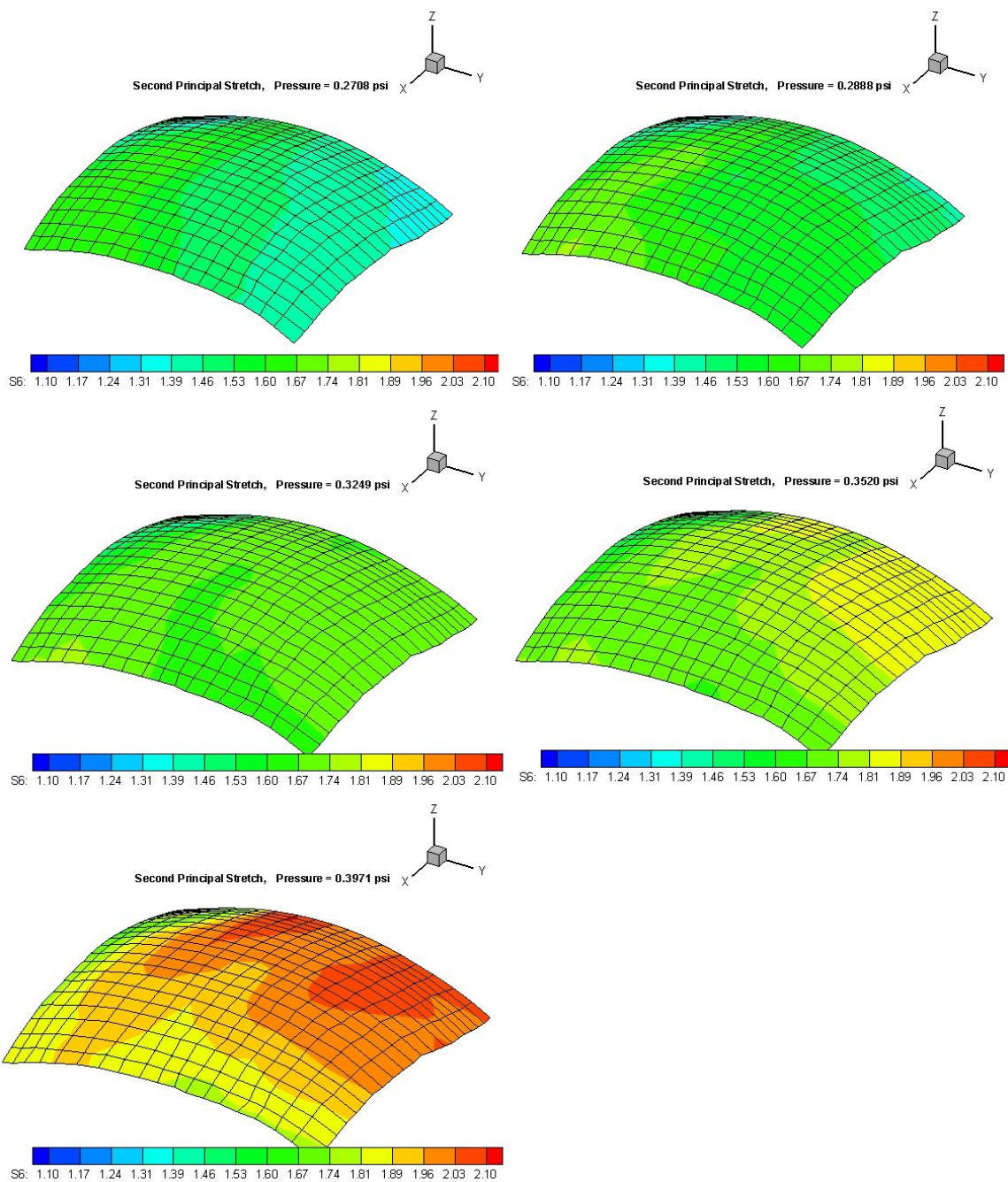


Figure D6. Second Principal Stretches, Pressure States 11 through 15.